11 STRONGLY INTERACTING HIGGS SECTOR AND ANOMALOUS COUPLINGS

11.1 Introduction

Georges Azuelos, Tao Han and Wolfgang Kilian

There is no fundamental principle that requires the physics responsible for electroweak symmetry breaking to be weakly interacting. In fact, there are many well-understood cases of spontaneous symmetry breaking in quantum physics, among them the breaking of electromagnetic gauge symmetry in superconductors and chiral symmetry breaking in QCD. In all these cases, the symmetry breaking is due to some interaction effectively becoming strong in a certain low-energy regime. In superconductors, this is the exchange of phonons near the Fermi surface. In QCD, the gluon coupling is effectively strong at energies below a GeV. These non-perturbative effects lead to a condensation of a field bilinear $\langle\psi\phi\rangle \neq 0$ which breaks the symmetry of the basic Lagrangian.

Mathematically, in such models of strong (dynamic) symmetry breaking the corresponding local operator $\psi\phi$ is a Higgs field. In general, the characteristics of the resulting Higgs boson will depend on the model. In QCD, for instance, the composite "Higgs" of chiral symmetry breaking is a heavy ($\sim$ GeV), poorly defined state. The lightest CP-even scalar, the broad $\sigma(600)$ meson resonance, may not even be thought of as a $q\bar{q}$ state [1] [cf. Section 12] and experimentally, its importance for low-energy hadronic interactions is minor compared to other states such as the ρ vector resonance. In QCD-like theories of electroweak symmetry breaking, the Higgs scalar is therefore expected to be very heavy and broad ($\sim$ TeV). In other dynamical theories, however, it can be associated with a low-lying excitation, such as in models with specific symmetry structure [cf. Section 7], or in technicolor theories with fermions in a higher dimensional represention of the gauge group [cf. Section 12]. Other conceivable mechanisms of electroweak symmetry breaking extend beyond four-dimensional quantum field theory. For instance, spontaneous symmetry breaking due to string interactions, bulk-brane interplay, or explicit symmetry-breaking boundary interactions in extra dimensions also could lead to a strongly-interacting effective field theory at the electroweak scale that need not involve Higgs-like states [cf. Section 10].

In this section, we consider first the scenario of electroweak symmetry breaking where the Higgs boson is either absent from the spectrum, or it is merely one among several heavy resonances, similar to the QCD case. In that case, strong interactions of some of the known particles are guaranteed in the TeV energy range. From the experience with QCD we can deduce that direct detection of the underlying new physics, analogous to quark-induced jets, may then need multi-TeV energies. However, even without a-priori knowledge of the underlying model we can nevertheless investigate the low-energy effective theory and identify observables that carry nontrivial information.

This could be the first information on the Higgs sector that becomes available through collider experiments at the LHC and the ILC.

We then consider the scenario where a light Higgs is present. The new physics, described by dimension-six operators of an effective Chiral Lagrangian, is then manifest, at high energy colliders, by anomalous couplings of the Higgs and Standard Model gauge bosons.

11.1.1 Weak interactions without a Higgs

In principle, it is trivial to write down the generic low-energy effective theory for a strongly interacting Higgs sector: this is simply the Standard Model (SM) with the physical Higgs field omitted. More precisely, we can formally remove the Higgs in the tree-level action by pushing its self-coupling in the potential to infinity, keeping the vacuum expectation value and all gauge and Yukawa couplings constant.

However, there is a tricky point with this approach. Since, in a generic gauge, the Higgs boson is part of a complex $SU(2)_L$ doublet together with the Goldstone bosons that provide the longitudinal components of the massive W and Z bosons, removing the Higgs also removes the gauge symmetry. The natural choice of removing the Higgs in unitarity gauge where Goldstone bosons do not appear,

results in an effective theory that does not exhibit any electroweak symmetry at all [2, 3]. This is a valid approach, but such a model does not naturally implement any of the well-established facts about electroweak symmetry, e.g., the left-handedness of charged currents, CKM unitarity for flavor mixing, or the W-Z mass relation.

Therefore, it is customary to construct the low-energy effective theory for electroweak interactions *bottom-up* by explicitly implementing gauge invariance [4–12]. In the absence of a Higgs boson, the $SU(2)_L \times U(1)_Y$ electroweak symmetry has then to be nonlinearly realized on the Goldstone-boson fields.

For the construction of the effective Lagrangian, let us introduce some notation. As building blocks we need the left-handed quark and lepton doublet fields (Q_L, L_L) and corresponding right-handed fields. For notational convenience, we also can write them as doublets (Q_R, L_R). Next, we introduce the Goldstone bosons of $SU(2)_L \times U(1)_Y \to U(1)_{\rm QED}$ spontaneous symmetry breaking, w^a $(a = 1, 2, 3)$ and their contraction with the Pauli matrices τ^a to a matrix-valued scalar field $\mathbf{w} = w^a\tau^a$. A possible nonlinear representation is realized by a derived matrix-valued scalar field of the form

$$\Sigma(x) = \exp\left(-\frac{i}{v}\mathbf{w}(x)\right), \tag{11.1}$$

where v is the electroweak constant $v = (\sqrt{2}\,G_F)^{-1/2} = 246\,\text{GeV}$. This field is required to transform as a $SU(2)_L$ doublet, transformations applied to the left. Local $U(1)_Y$ (hypercharge) transformations apply as $\Sigma \to \Sigma\exp(i\beta(x)\,\tau^3/2)$. Note that Σ is a unitary matrix $(\Sigma^\dagger\Sigma = 1)$, and electroweak transformations act linearly on $\Sigma(x)$, but nonlinearly on $\mathbf{w}(x)$.

The electroweak gauge boson fields are W^a_μ $(a = 1, 2, 3)$ and B_μ, which we contract with the Pauli matrices τ^a to matrix-valued vector fields $\mathbf{W}_\mu = W^a_\mu\tau^a/2$ and $\mathbf{B}_\mu = \Sigma B_\mu(\tau^3/2)\Sigma^\dagger$. In accordance with the gauge transformation properties, the covariant derivative of Σ is

$$\mathbf{D}_\mu\Sigma = (i\partial_\mu + g\mathbf{W}_\mu - g'\mathbf{B}_\mu)\Sigma. \tag{11.2}$$

The covariant derivatives of fermion fields involve the corresponding representation matrices of the $SU(2)_L \times U(1)_Y$ symmetry, which differ between left- and right-handed fermions. We also need field-strength tensors

$$\mathbf{W}_{\mu\nu} = \partial_\mu\mathbf{W}_\nu - \partial_\nu\mathbf{W}_\mu + ig[\mathbf{W}_\mu, \mathbf{W}_\nu] \qquad \text{and} \qquad \mathbf{B}_{\mu\nu} = \partial_\mu\mathbf{B}_\nu - \partial_\nu\mathbf{B}_\mu. \tag{11.3}$$

Finally, it is convenient to introduce two covariant fields derived from Σ, a vector and a scalar:

$$\mathbf{V}_\mu = \Sigma(\mathbf{D}_\mu\Sigma^\dagger), \qquad \mathbf{T} = \Sigma\tau^3\Sigma^\dagger. \tag{11.4}$$

With these definitions, the generic low-energy effective Lagrangian for the electroweak interactions of leptons, quarks, and gauge bosons is

$$\begin{aligned}\mathcal{L} = {} & -\frac{1}{2}\,\text{tr}[\mathbf{W}_{\mu\nu}\mathbf{W}^{\mu\nu}] - \frac{1}{2}\,\text{tr}[\mathbf{B}_{\mu\nu}\mathbf{B}^{\mu\nu}] + \frac{v^2}{4}\,\text{tr}[(\mathbf{D}_\mu\Sigma)(\mathbf{D}^\mu\Sigma)^\dagger] - \beta'\frac{v^2}{8}\,\text{tr}[\mathbf{T}\mathbf{V}_\mu]\,\text{tr}[\mathbf{T}\mathbf{V}^\mu] \\ & + \bar{Q}_L i\not{D} Q_L + \bar{Q}_R i\not{D} Q_R + \bar{L}_L i\not{D} L_L + \bar{L}_R i\not{D} L_R \\ & - (\bar{Q}_L\Sigma M_Q Q_R + \bar{L}_L\Sigma M_L L_R + \text{h.c.}) - \bar{L}^c_L\Sigma^* M_{N_L}\frac{1+\tau^3}{2}\Sigma L_L - \bar{L}^c_R M_{N_R}\frac{1+\tau^3}{2}L_R \\ & + \cdots,\end{aligned} \tag{11.5}$$

where we wrote only the operators with the lowest dimension. In this Lagrangian, QED (and, implicitly, QCD) gauge invariance is still linearly realized.

Before continuing, let us add a few remarks on this Lagrangian: (i) the particular representation of Σ in terms of $\mathbf{w}$ is irrelevant, only the symmetry properties matter; (ii) the unitarity gauge is recovered

by $\mathbf{w} \equiv 0$, i.e., $\Sigma \equiv 1$, and yields a Lagrangian identical to the Standard Model with Higgs removed; (iii) we could write Majorana and Dirac masses for both left- and right-handed neutrinos.

The Lagrangian (11.5) uniquely determines the leading term in a low-energy expansion of all scattering amplitudes. The W and Z masses result from the first term in the Σ expansion,

$$M_W = gv/2 \qquad \text{and} \qquad M_Z = \sqrt{g^2 + g'^2}(1 + \beta'/2)\, v/2 \tag{11.6}$$

The experimental results imply that the ρ parameter, related to the coefficient β', vanishes at tree level [1], hence $\beta' = 0$. This is understood as an extra $SU(2)_R$ symmetry of the dimension-2 part of the (bosonic) Lagrangian, called *custodial* symmetry [13–16]. It is often assumed to be an approximate symmetry of the fundamental physics responsible for electroweak symmetry breaking, even though there are further parameters in the tree-level Lagrangian that break the symmetry explicitly, most notably g' and m_t.

This effective theory is formally non-renormalizable. While the Lagrangian already contains an infinite number of terms with prefactor $1/v^n$ due to the infinite series expansion of Σ, computing radiative corrections requires another infinite series of higher-dimensional counterterms, indicated by dots in (11.5). These extra counterterms carry prefactors $1/(4\pi v)^n$ and are therefore suppressed. Below energies of about $4\pi v = 3\,\mathrm{TeV}$ the effective theory has some region of applicability. Above that scale, it has no physical content anymore.

In addition to counterterms, we can add extra contributions to higher-dimensional operators with arbitrary coefficients. Within a specific underlying strong-interaction model we expect the actual coefficients, computed in a given renormalization scheme, to be well-defined. A similar program, set up for low-energy hadronic interactions, has proven very successful [4, 17, 18], and is currently used as a convenient gauge for lattice QCD calculations. In the electroweak case, the list of CP-even dimension-4 bosonic operators reads [7, 8]

$$\mathcal{L}_1 = \alpha_1 g g' \,\mathrm{tr}[\mathbf{B}_{\mu\nu}\mathbf{W}^{\mu\nu}], \qquad \mathcal{L}_6 = \alpha_6 \,\mathrm{tr}[V_\mu V_\nu]\,\mathrm{tr}[\mathbf{T}V^\mu]\,\mathrm{tr}[\mathbf{T}V^\nu], \tag{11.7}$$

$$\mathcal{L}_2 = i\alpha_2 g' \,\mathrm{tr}[\mathbf{B}_{\mu\nu}[V^\mu, V^\nu]], \qquad \mathcal{L}_7 = \alpha_7 \,\mathrm{tr}[V_\mu V^\mu]\,\mathrm{tr}[\mathbf{T}V_\nu]\,\mathrm{tr}[\mathbf{T}V^\nu], \tag{11.8}$$

$$\mathcal{L}_3 = i\alpha_3 g \,\mathrm{tr}[\mathbf{W}_{\mu\nu}[V^\mu, V^\nu]], \qquad \mathcal{L}_8 = \tfrac{1}{4}\alpha_8 g^2 (\mathrm{tr}[\mathbf{T}\mathbf{W}_{\mu\nu}])^2, \tag{11.9}$$

$$\mathcal{L}_4 = \alpha_4 (\mathrm{tr}[V_\mu V_\nu])^2, \qquad \mathcal{L}_9 = \tfrac{i}{2}\alpha_9 g \,\mathrm{tr}[\mathbf{T}\mathbf{W}_{\mu\nu}]\,\mathrm{tr}[\mathbf{T}[V^\mu, V^\nu]], \tag{11.10}$$

$$\mathcal{L}_5 = \alpha_5 (\mathrm{tr}[V_\mu V^\mu])^2, \qquad \mathcal{L}_{10} = \tfrac{1}{2}\alpha_{10} (\mathrm{tr}[\mathbf{T}V_\mu]\,\mathrm{tr}[\mathbf{T}V_\nu])^2, \tag{11.11}$$

$$\mathcal{L}_{11} = \alpha_{11} g \epsilon^{\mu\nu\rho\lambda} \,\mathrm{tr}[\mathbf{T}V_\mu]\,\mathrm{tr}[V_\nu \mathbf{W}_{\rho\lambda}]. \tag{11.12}$$

CP-odd operators, operators involving fermions, and higher-dimensional terms may be added to this list, but are not considered in most studies.

In the above list, the coefficients α_i are dimensionless. As long as the operators are generated only as counterterms, their coefficients are naturally of order $1/16\pi^2$; for this reason, a different normalization that multiplies the coefficients by $16\pi^2$ is used frequently in the literature. Additional contributions due to new physics can in principle be of arbitrary magnitude, but in a strong-interaction scenario they tend to be somewhat larger than the loop contributions. Higher-dimensional terms, which we do not consider at this point, would be suppressed by additional factors of $1/(4\pi v)^2$.

Due to the fact that $\beta' = 0$ at tree level, bosonic loops generate those operators that involve $\mathbf{T}$ factors only with coefficients suppressed by g'^2, the small hypercharge coupling squared. Nevertheless, these terms may be present in the tree-level Lagrangian with unsuppressed coefficients. Loops involving top quarks also break the custodial symmetry.

11.1.2 Vector-Boson Scattering

Despite the fact that the use of the effective Chiral Lagrangian is limited to the range up to a few TeV, it is nevertheless a valuable tool since this is exactly the energy range that will be accessed by the upcoming

LHC and ILC colliders. The bilinear couplings α_1 and α_8, related to the S and T parameters [19, 20], have already been measured at LEP1 in 2-fermion production [1, 21]. For the trilinear couplings $\alpha_2, \alpha_3, \alpha_9, \alpha_{11}$, 4-fermion processes ($W$ pair and single-W or single-Z production) are needed [21–23] There was some sensitivity at LEP2, but in order to reach the order of magnitude $\alpha_i \sim 1/16\pi^2$ implied by the perturbative expansion, LHC and ILC data will be necessary [24–27]. Finally, the remaining couplings are accessed at the LHC [28–33] and the ILC [27, 34–38] by 6-fermion processes (Fig. 11.1). Since the 4-fermion processes also depend on the anomalous two-boson couplings, and the 6-fermion processes also depend on all lower-order couplings, in practice a simultaneous fit of all couplings is necessary to extract their physical values.

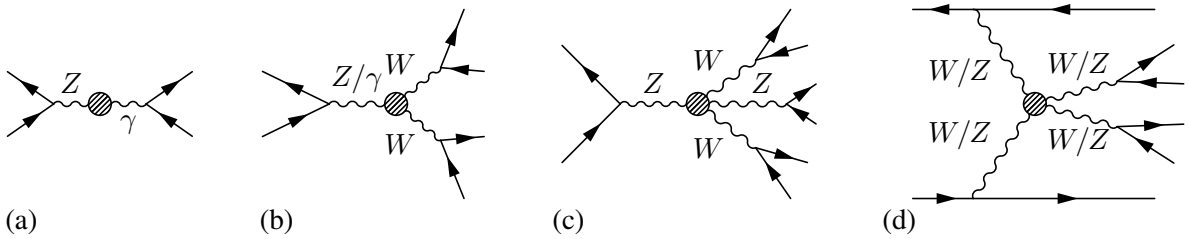

Fig. 11.1: Processes that involve the anomalous couplings (a) $\alpha_{1,8}$; (b) $\alpha_{2,3,9,11}$; (c,d) $\alpha_{4,5,6,7,10}$, respectively. The fermions may be either quarks or leptons.

The 6-fermion processes of type Fig. 11.1d are of particular interest, since in the limit that the intermediate vector bosons get on-shell, they include $2 \to 2$ quasi-elastic vector boson scattering as subprocesses. (Processes of type Fig. 11.1c probe the same interactions in a far off-shell regime.) These are the only accessible $2 \to 2$ processes[1] that contain the Higgs, if it exists, at tree-level. Consequently, the absence of a Higgs boson has a strong effect: quasi-elastic vector-boson scattering amplitudes, as calculated at lowest order, rise without bound and surpass their unitarity limit in the TeV range [42, 43]. Higher-order corrections would remedy this, but depend on the unknown infinite series of higher-order counterterms and thus leave the actual result undetermined. Observing the presence or absence of strong interactions in 6-fermion production is thus the ultimate experimental test of the Higgs mechanism, independent of its particular realization: strong interactions are absent if light scalar state(s) are present in the model and couple exactly as required by the constraint that the symmetry is broken exclusively by their vacuum expectation value(s).

For quantitative estimates, it is convenient to start with the limit $g, g', m_f \to 0$ (but v constant), where the gauge symmetry is formally broken, but the gauge-boson and fermion masses are arbitrarily small. In this limit, several simplifications apply to the processes of type Fig. 11.1d: (i) the final-state gauge bosons can be treated in the narrow-width approximation; (ii) the initial-state gauge bosons are approximately on-shell and can, at small angles, be treated as partons within the incoming fermions: the Effective W Approximation [44–46]; (iii) the scattering amplitudes of longitudinally polarized vector bosons become equal to corresponding scattering amplitudes of Goldstone bosons, while the transversal degrees of freedom decouple: the Goldstone-boson Equivalence Theorem [47–49]; (iv) the resulting Lagrangian is exactly identical to the effective Lagrangian of low-energy pion scattering in the $m_\pi \to 0$ limit: Chiral Perturbation Theory [4, 17, 18].

The last analogy allows us to transfer QCD knowledge to the present case. Noting that the scattering amplitudes of transversal gauge bosons do not violate unitarity limits, we conclude that the dominant contributions to quasi-elastic vector boson scattering amplitudes fulfil, like pion scattering amplitudes, $SU(2)$ symmetry relations. We can diagonalize the $2 \to 2$ scattering matrix and derive the strongest bound on the low-energy effective theory: The amplitude projected onto $J = 0$ (angular momentum) and $I = 0$ (weak isospin) saturates the unitarity limit at $E = \sqrt{8\pi}\, v = 1.2\,\mathrm{TeV}$ [42, 43]. Due to the

[1] with the exception of vector-boson scattering into heavy-quark pairs [39–41], which however is an experimental challenge.

rapidly falling W/Z structure functions, the c.m. energy of the incoming fermions has to be considerably above that limit if this unitarity saturation is to have an observable effect.

In the actual environment of the LHC and ILC colliders with their limited energy reach, cuts and backgrounds, it turns out that these estimates in the gaugeless limit are useful for qualitative considerations, but fail if reasonably precise values for cross sections and simulated event samples are desired. Dropping the approximations (i) to (iv) above altogether, the physical picture becomes much less clear; in particular, the implications of unitarity saturation for the complete off-shell process are not obvious. While at the ILC it is unlikely that the unitarity limit can be reached, the kinematic capability of the LHC does extend into that range. However, the high background and the rapidly falling structure functions make it a challenge also at the LHC to detect observable consequences of unitarity violation in a naive tree-level extrapolation. Therefore, the Chiral Lagrangian (11.5), optionally augmented by resonances coupled with free coefficients, is a theoretical framework sufficient for all practical purposes. As a consequence, while we are not allowed to use simplifying approximations in calculating the 6-fermion processes of interest at the LHC or the ILC, with appropriate calculational tools it is possible to make reliable predictions and to compare them with data.

11.1.3 Low-Energy Parameters

Without any knowledge about the underlying mechanism that triggers electroweak symmetry breaking, we have no idea about how the scattering amplitudes will evolve beyond the limit where the effective theory fails. At least, the α parameters allow us to parameterize scattering amplitudes, and once data are available, values for the parameters can be obtained. For the ILC studies, we essentially have a complete picture about the possible sensitivity on the α couplings [27,50,51] which involves a complete simulation of the 6-fermion process and does not rely on further simplifying assumptions at the theoretical level. For isolating the strong scattering signal, one looks at four-jet events in association with missing energy due to the forward-scattered neutrinos or electrons in the final state. The main uncertainties originate from the ambiguity in identifying W and Z bosons in their hadronic decay modes, which for the current detector designs appears to be manageable. These results currently include all known backgrounds and detector effects based on fast simulation.

11.1.4 Resonances

It is likely that WW scattering amplitudes do not just saturate unitary and remain featureless at higher energies. Just like in the analogous situation of $\pi\pi$ scattering, there may be strong resonances on top of that which could be observable at the LHC at energies above the $1.2\,\mathrm{TeV}$ cutoff. The best-studied cases are (i) a heavy scalar, or (ii) a heavy vector. The first case is just the heavy-mass extrapolation of the Standard Model, while the second one is modelled after the QCD case with its strong ρ resonances [52–54].

It should be kept in mind, however, that the actual situation may be very different. For instance, in the context of models that entangle electroweak symmetry with extra dimensions and gravitation, tensor resonances could play an important role. So far, a few studies have considered the prospects for distinguishing qualitatively different scenarios at hadron and lepton colliders [28–30], and for the case of vector resonances, the possibility of resonance parameter measurements have been discussed. An experimental analysis of the general case that would allow for quantitative conclusions on all possible resonance couplings is desirable, but so far has not been attempted. In the ILC context, a detailed study that relates the estimated uncertainties of anomalous coupling measurements to the coupling parameters of heavy resonances can be found in [51] (see also Section 11.2).

Without a preferred underlying model, extrapolating the scattering amplitudes of vector bosons beyond the range where the lowest-order prediction saturates unitarity remains speculative. There exists an infinite set of extrapolation prescriptions that, at least, maintain elastic unitarity. Particularly popular

are the K-matrix model [55, 56] that parameterizes featureless amplitudes (resonant at infinity), and the Padé or inverse-amplitude method [57, 58] that parameterizes in each channel, up to the order where it is typically evaluated, a single resonance with a specified mass and coupling strength. The latter method has proven successful in the description of low-energy QCD amplitudes [59]; this success is due to the particular property of QCD to contain dominant resonances in its hadron form factors and scattering amplitudes. Adopting this unitarization prescription and making further assumptions such as custodial symmetry, with which vector boson scattering is determined by the only coefficients α_4 and α_5, resonances can be mapped in two-dimensional parameter space [58]. Unfortunately, despite the good description of QCD amplitudes by such a model, we have no clue whether a strong-interaction theory of electroweak interactions would actually exhibit such a behavior.

LHC studies [30, 32, 33, 58, 60–62] on prospects for observing vector boson scattering remain at the parton or fast detector simulation level, but full detector simulation analyses are in progress. They generally rely on the abovementioned simplifying assumptions, and should therefore not be taken at face value. The results are valid, however, for a generic resonance and can be re-interpreted in the context of a more general Chiral Lagrangian model. They could serve, in principle, to derive limits on the α couplings. The WZ scattering signal, with one or two leptons in the final state, can be observed up to a mass of ~ 1500 GeV [60] within a few years of LHC running at nominal luminosity (see Fig. 11.2). The major irreducible background is $WZjj$ from SM processes involving gluon or γ/Z exchange diagrams, with transversely polarized vector bosons radiated from incoming or outgoing quarks. It has been shown [63, 64] that a complete description of the 6-fermion process is necessary for a correct evaluation of vector boson scattering. The reducible backgrounds are $t\bar{t}$ production and $W + j$ or $Z + j$, which have all very high cross sections. Using either the Padé or N/D unitarization protocol, it has also been shown [33] that scalar and vector resonances may occur in the channel $WW \rightarrow jj + \ell\nu$ in the TeV region and if so, should be observable at the LHC. In all cases, the requirement of forward jets, expected to result from the outgoing primary quarks in Fig. 11.1d, and of a veto on an excess of central jets is essential for an effective reduction of these backgrounds.

The BESS model [52, 53] (which stands for *Breaking Electoweak Symmetry Strongly*) is another general framework for describing resonances in gauge boson scattering. The model is without a Higgs, but with a triplet of new massive QCD-like vector bosons V. These bosons are originally auxiliary fields of a hidden SU(2) symmetry, but it is explicitly assumed that they become physical and a kinetic term is added for them. The new $V^{\pm,0}$ bosons mix with the W and Z of the SM through a mixing angle proportional to $x = g/g''$, where g'' is the self-coupling of the V. Another parameter, b, governs the coupling to fermions. A variant of this model, called the degenerate BESS model [65, 66], predicts the existence of two triplets of new gauge bosons $L^{\pm}, L_3, R^{\pm}, R_3$ which are almost degenerate in mass, the mass splitting depending on the above parameter x, and with the neutral bosons mixing with the SM electroweak boson. The BESS models could be an effective theory for which walking type technicolor theories (see Section 12) are possible prototypes of an underlying gauge theory [67,68]. Expected bounds on the parameters of the BESS model can be found in [27]. The degenerate model is best studied in the $f\bar{f}$ decay channels of the new resonances. Expected 95% limits in the parameter space $\{x, M\}$ in present and future colliders are given in [69, 70], where it is shown that with 100 fb^{-1}, the LHC can discover resonances up to $\sim$ 2 TeV, for $x = 0.1$, and that CLIC could measure the width, mass, double peak structure and forward-backward asymmetries around the L_3 and R_3 resonances. A CMS study [71] has investigated in detail the discovery reach for the channel decaying to muons.

11.1.5 Weak interactions with a Higgs

While the effective Lagrangian (11.5) may be obtained as the heavy-Higgs limit of the Standard Model, the reverse construction can also be made: we may introduce a CP-even neutral scalar resonance h and couple it to any of the terms in (11.5) with a-priori arbitrary strength. This case is covered by the resonance studies mentioned above. If we make the particular choice of replacing Σ by $(1 + h/v)\Sigma$ in all of

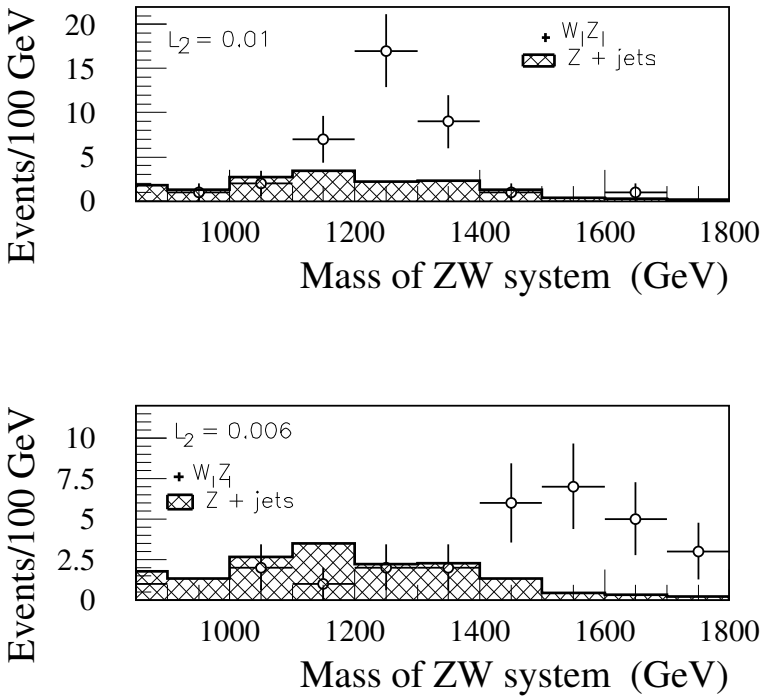

Fig. 11.2: Reconstructed mass distribution the $WZ \to jj\ \ell\ell$ system for different assumed resonance masses, and for an integrated luminosity of 300 fb^{-1}. The background shown is Z + jets. Fast detector simulation was used. (from ref [60])

its explicit occurences, and add some specific scalar self-couplings, we can apply a nonlinear field redefinition and transform the Chiral Lagrangian coupled to the resonance h into the usual Standard Model. Since nonlinear field redefinitions, with proper renormalizations of higher-dimensional counterterms, do not affect the S-matrix, one thus proves that the Chiral Lagrangian coupled to a scalar in a specific way is exactly equivalent to the Standard Model. This also means that a fictitious heavy Higgs boson is equivalent to a formal cutoff for the extra loop divergences and, conversely, a cutoff can be interpreted as an effective Higgs mass.

If the Higgs state is sufficiently light such that the linear realization of the Chiral Lagrangian appears appropriate as a theoretical framework, we should revise the power-counting implicit in our previous discussion. After the appropriate nonlinear redefinition of h and $\mathbf{w}$ that turns a generic parameterization into the linear representation, we may consider the resulting matrix field

$$H = v(1 + h/v)\Sigma = (v + h')\mathbf{1} - i\mathbf{w}' \tag{11.13}$$

as a canonical scalar multiplet with mass dimension 1 and vacuum expectation value $\langle H \rangle = v\mathbf{1}$ that can alternatively be decomposed in terms of column vectors $\tilde{\Phi}, \Phi$ with $\tilde{\Phi} = i\tau^2\Phi^*$:

$$H = \begin{pmatrix} v + h - iz & -i\sqrt{2}w^+ \\ -i\sqrt{2}w^- & v + h + iz \end{pmatrix} = \sqrt{2}\begin{pmatrix} \tilde{\Phi} & \Phi \end{pmatrix}. \tag{11.14}$$

Rewriting everything in terms of the complex doublet Φ, the lowest-order terms of the Chiral Lagrangian turn into the textbook expression for the SM Lagrangian.

There is no reason to discard the possibility of anomalous couplings in this linear realization, where the dimensionality of the operators is modified. Eliminating factors $\Sigma^\dagger\Sigma = 1$ as far as possible before the transformation to the linear representation is made, in (11.5) we thus assign dimension 6 to

the operators multiplying β' and M_{N_L}, dimension 4 to the kinetic energy of Σ, replaced by H, while only the operator multiplying M_{N_R} retains dimension 2. In the list (11.7–11.12), the operators $\mathcal{L}_{1,2,3}$ are assigned dimension-6, $\mathcal{L}_{4,5,9,11}$ become dimension-8, and the others acquire even higher canonical dimension. Furthermore, at the level of dimension-6 operators we have to include four-fermion operators and additional terms that involve vector bosons and the Higgs field; various operator bases and detailed discussions can be found in Refs. [72–79].

Conventionally, the effective interactions are parameterized as

$$\mathcal{L}_{\text{eff}} \;=\; \sum_n \frac{f_n}{\Lambda^2}\mathcal{O}_n\,, \tag{11.15}$$

where f_n's are dimensionless "anomalous couplings", and $\mathcal{O}_n$ the gauge-invariant dimension-6 operators, constructed from the SM fields. If Λ appropriately parameterizes the new physics scale (such as the mass of the next resonance), then one would expect f_n's to be of the order of unity. The anomalous couplings of the Higgs boson and gauge bosons are of special interest since they may be directly related to the mechanism of EWSB. A possible parameterization of the C and P conserving dimension-6 effective operators of our current interests involving the $SU(2)$ gauge field W^i_μ, the $U(1)$ gauge field B_μ as well as a Higgs doublet h is given by

$$\mathcal{O}_{BW} = \Phi^\dagger \hat{B}_{\mu\nu}\hat{W}^{\mu\nu}\Phi, \qquad \mathcal{O}_{\Phi,1} = \left(D_\mu\Phi\right)^\dagger \Phi^\dagger\Phi \left(D^\mu\Phi\right), \tag{11.16}$$

$$\mathcal{O}_{\Phi,2} = \frac{1}{2}\partial^\mu\left(\Phi^\dagger\Phi\right)\partial_\mu\left(\Phi^\dagger\Phi\right), \qquad \mathcal{O}_{\Phi,3} = \frac{1}{3}\left(\Phi^\dagger\Phi\right)^3, \tag{11.17}$$

$$\mathcal{O}_W = (D_\mu\Phi)^\dagger\hat{W}^{\mu\nu}(D_\nu\Phi), \qquad \mathcal{O}_B = (D_\mu\Phi)^\dagger\hat{B}^{\mu\nu}(D_\nu\Phi),$$

$$\mathcal{O}_{WW} = \Phi^\dagger\hat{W}_{\mu\nu}\hat{W}^{\mu\nu}\Phi, \qquad \mathcal{O}_{BB} = \Phi^\dagger\hat{B}_{\mu\nu}\hat{B}^{\mu\nu}\Phi, \tag{11.18}$$

where $\hat{B}_{\mu\nu}$ and $\hat{W}_{\mu\nu}$ stand for

$$\hat{B}_{\mu\nu} = i\frac{g'}{2}B_{\mu\nu}, \qquad \hat{W}_{\mu\nu} = i\frac{g}{2}\tau^a W^a_{\mu\nu},$$

in which g and g' are the $SU(2)$ and $U(1)$ gauge couplings, respectively.

Precision electroweak data and the measurements of the triple-gauge-boson couplings give considerable constraints on some of the anomalous couplings f_n/Λ^2 [78–80]. For instance, the oblique correction parameters S and T [19] give rise to constraints on the anomalous coupling constants f_{BW} and $f_{\Phi,1}$ in Eq. (11.16). Assuming either f_{BW} or $f_{\Phi,1}$ dominance, the 2σ constraints obtained are quite strong [80],

$$-0.07 < \frac{f_{BW}}{(\Lambda/\text{TeV})^2} < 0.04, \quad -0.02 < \frac{f_{\Phi,1}}{(\Lambda/\text{TeV})^2} < 0.02.$$

At the LHC, considerably improved bounds on anomalous triple gauge boson couplings can be expected [24], with 30 fb^{-1}. Systematic errors arise from higher order QCD contributions to vector boson pair production [81], and from uncertainties in parton distibution functions. These couplings, expressed as energy dependent form factors in order to safe-guard unitarity, are related [76] to f_W, f_B given above, as well as f_{WWW}. A study of the LHC sensitiviy to anomalous quartic couplings is in progress [82]

The next two operators in Eq. (11.17) are purely Higgs boson self-interactions, and lead to corrections to the Higgs triple and quartic vertices. They have been dedicatedly studied in [79] at linear colliders and we will not pursue them further. However, the present experimental observables are not sensitive to the four anomalous coupling operators O_W, O_{WW}, O_B and O_{BB} (with anomalous coupling constants f_W/Λ^2, f_{WW}/Λ^2, f_B/Λ^2 and f_{BB}/Λ^2) in Eq. (11.18). The constraints from the existing experiments and the requirement of unitarity of the S matrix element on these four anomalous coupling constants are

Table 11.1: Current 2σ constraints on f_n/Λ^2 from existing studies. The results are obtained by assuming that only one anomalous coupling is nonzero at a time.

Constraints from	f_n/Λ^2 in TeV^{-2}
Precision EW fit [80]:	$-6 \leq \frac{f_W}{\Lambda^2} \leq 5$
	$4.2 \leq \frac{f_B}{\Lambda^2} \leq 2.0$
	$-5.0 \leq \frac{f_{WW}}{\Lambda^2} \leq 5.6$
	$17 \leq \frac{f_{BB}}{\Lambda^2} \leq 20$
Triple gauge couplings [78]	$-31 \leq \frac{f_W+f_B}{\Lambda^2} \leq 68$
LEP2 Higgs searches [83]:	$-7.5 \leq \frac{f_{WW(BB)}}{\Lambda^2} \leq 18$
Unitarity (at $\sqrt{s}$=2 TeV) [84, 85]:	$\lvert\frac{f_B}{\Lambda^2}\rvert \leq 24.5; \quad \lvert\frac{f_W}{\Lambda^2}\rvert \leq 7.8$
	$-160 \leq \lvert\frac{f_{BB}}{\Lambda^2}\rvert \leq 197; \quad \lvert\frac{f_{WW}}{\Lambda^2}\rvert \leq 39.2$

rather weak. We summarize the above constraints on those four anomalous couplings in Table 11.1. The results are obtained by assuming that only one anomalous coupling is nonzero at a time.

It is perhaps more intuitive to express the new operators in terms of couplings of the explicit physical component fields. Taking into account of the mixing between W_μ^3 and B_μ, the effective couplings of the Higgs boson H and the electroweak gauge bosons V ($V = \gamma,\ W^\pm,\ Z$) in Eq. (11.18) can be cast into [78]

$$\begin{aligned}\mathcal{L}_{\text{eff}}^H &= g_{H\gamma\gamma} H A_{\mu\nu} A^{\mu\nu} + g_{HZ\gamma}^{(1)} A_{\mu\nu} Z^\mu \partial^\nu H + g_{HZ\gamma}^{(2)} H A_{\mu\nu} Z^{\mu\nu} + g_{HZZ}^{(1)} Z_{\mu\nu} Z^\mu \partial^\nu H \\ &\quad + g_{HZZ}^{(2)} H Z_{\mu\nu} Z^{\mu\nu} + g_{HWW}^{(1)} (W_{\mu\nu}^+ W^{-\mu} \partial^\nu H + \text{h.c.}) + g_{HWW}^{(2)} H W_{\mu\nu}^+ W^{-\mu\nu}, \quad (11.19)\end{aligned}$$

where the anomalous couplings g_{HVV}'s (of dimension -1) are related to those Lagrangian parameters f_n's by

$$\begin{aligned} g_{H\gamma\gamma} &= -\alpha \frac{s^2 (f_{BB} + f_{WW})}{2}, \\ g_{HZ\gamma}^{(1)} &= \alpha \frac{s(f_W - f_B)}{2c}, \qquad g_{HZ\gamma}^{(2)} = \alpha \frac{s[s^2 f_{BB} - c^2 f_{WW}]}{c}, \\ g_{HZZ}^{(1)} &= \alpha \frac{c^2 f_W + s^2 f_B}{2c^2}, \qquad g_{HZZ}^{(2)} = -\alpha \frac{s^4 f_{BB} + c^4 f_{WW}}{2c^2}, \\ g_{HWW}^{(1)} &= \alpha \frac{f_W}{2}, \qquad\qquad g_{HWW}^{(2)} = -\alpha f_{WW}, \end{aligned} \quad (11.20)$$

with the weak mixing $s \equiv \sin\theta_W,\ c \equiv \cos\theta_W$ and $\alpha = g M_W/\Lambda^2 \approx 0.053\ \text{TeV}^{-1} \approx 1/(19\ \text{TeV})$ for $\Lambda = 1$ TeV . Roughly speaking, an order unity coupling of f_n translates to $g_{HVV}^{(i)} \sim 1/(20\ \text{TeV})$=0.05 TeV^{-1}.

Since new physics responsible for the mechanism of the EWSB is more likely to show up with the Higgs couplings to gauge bosons, these couplings should be tested as thoroughly as possible at future high energy colliders. At the LHC the most sensitive constraints on f_W/Λ^2 and f_{WW}/Λ^2 will be from the measurement of the gauge-boson scattering $W^+W^+ \to W^+W^+$ [80]. The obtained 2σ level constraints on these two anomalous couplings are

$$-1.4\ \text{TeV}^{-2} < f_W/\Lambda^2 < 1.2\ \text{TeV}^{-2}, \quad \text{and} \quad 2.2\ \text{TeV}^{-2} \leq f_{WW}/\Lambda^2 < 2.2\ \text{TeV}^{-2}, \quad (11.21)$$

which may reach the parameter regime sensitive to TeV-scale new physics. Those processes are insensitive to f_B/Λ^2 and f_{BB}/Λ^2 however. At the e^+e^- linear colliders on the other hand, the anomalous couplings $g^{(1)}_{HZZ}$ and $g^{(2)}_{HZZ}$ can be constrained at the 2σ sensitivity to $(10^{-3} - 10^{-2})$ TeV^{-1} from the Higgs-strahlung process $e^+e^- \to Z^* \to ZH$ [86–91].

Due to the renormalizability of the dimension-4 part of the SM effective Lagrangian, there is no a-priori limit on the prefactors multiplying the higher-dimensional operators $1/\Lambda^n$: the cutoff Λ may be arbitrarily high. However, the naturalness problem of the Higgs self-energy (an uncancelled quadratic divergence that would imply strong fine-tuning for high cutoff Λ) lets us argue that Λ is nevertheless in the TeV range or below, and new particles or interactions should be expected there that induce anomalous couplings at the same level as in the nonlinear Higgs-less representation. From the power-counting in the linear realization we may draw the qualitative conclusions that custodial symmetry is approximately conserved (since β' now multiplies a dimension-6 operator), that the Majorana mass parameters of right-handed neutrinos are large (M_{N_R} multiplying a dimension-2 operator), effectively removing right-handed neutrinos from the low-energy spectrum, and that the Majorana mass parameters M_{N_L} of left-handed neutrinos are small (dimension-6). These properties are apparently realized in Nature and therefore provide some support for the light-Higgs hypothesis.

In weakly-interacting extensions of the SM (e.g., Little-Higgs models), some combinations of the anomalous coefficients can be induced at tree-level and are thus suppressed by factors of v^2/Λ^2, while the rest requires loops and is thus suppressed by additional factors $1/16\pi^2$. In particular, in models where all extra low-lying particles carry a conserved parity quantum number (e.g., the MSSM, Little-Higgs models with T-parity, universal extra dimensions), anomalous couplings have a common suppression of at least $v^2/(16\pi^2\Lambda^2)$ and are very difficult to detect. This could be an explanation of the absence of deviations from the SM in the precision data obtained so far. However, the list of anomalous couplings has not been exhausted by previous measurements, and precise data from LHC and ILC will be necessary to complete the picture.

11.2 Anomalous quartic gauge couplings at the ILC

Michael Beyer, Wolfgang Kilian, Predrag Krstonošić, Klaus Mönig, Jürgen Reuter, Erik Schmidt and Henning Schröder

A measurement of quasi-elastic vector boson scattering, i.e., of quartic gauge couplings, is clearly the most direct probe of the Higgs mechanism. In this subsection we present a new determination of the sensitivity the ILC can provide for the couplings $\alpha_{4,5,6,7,10}$ that modify the quartic gauge couplings. Furthermore, we translate this sensitivity into the physics reach for new resonances that could be responsible for such anomalous couplings. Details of the study can be found in Ref. [51].

11.2.1 Analysis of triple weak-boson production

We first consider the triple gauge-boson production processes $e^+e^- \to W^+W^-Z$ and $e^+e^- \to ZZZ$. In these processes not all anomalous couplings can be disentangled individually. The process $e^+e^- \to W^+W^-Z$ depends on the α parameters in the two linear combinations $\alpha_4 + \alpha_6$ and $\alpha_5 + \alpha_7$, while the process $e^+e^- \to ZZZ$ depends on the single combination $\alpha_4 + \alpha_5 + 2(\alpha_6 + \alpha_7 + \alpha_{10})$. For the study of triple gauge-boson production we concentrate on α_4 and α_5 as independent couplings.

The total cross section at $\sqrt{s} = 1000$ GeV as calculated with the event generator `WHIZARD` [92] is given in Table 11.2. For the analysis presented here, we produce SM events corresponding to a luminosity of 1000 fb^{-1}. Three-boson events are reconstructed via six (hadronic) jets utilizing the YCLUS jet-finding algorithm with the Durham recombination scheme. The dominant background is due to $t\bar{t} \to b\bar{b}WW \to 6$ jets. We select events with kinematical conditions for a combination of missing energy and transverse momentum and combine jets to form a W or a Z by requiring a window in invariant mass

Table 11.2: Cross section for triple boson production at $\sqrt{s} = 1000\,\mathrm{GeV}$ for different initial state polarization. (A) unpolarized, (B) 80%R electrons, and (C) 80%R electrons with 60%L positrons.

WWZ			ZZZ
no pol.	e^-pol.	both pol.	no pol.
59.1 fb	12.3 fb	5.57 fb	0.79 fb

Table 11.3: Sensitivity of α_4 and α_5 expressed as 1σ errors. WWZ: two-parameter fit; ZZZ: one-parameter fit; best: best combination of both. Positive (σ^+) and negative (σ^-) errors are given separately.

		WWZ			ZZZ	best
		no pol. (case A)	e^- pol. (case B)	both pol. (case C)	no pol.	
$16\pi^2\Delta\alpha_4$	σ^+	9.79	4.21	1.90	3.94	1.78
	σ^-	-4.40	-3.34	-1.71	-3.53	-1.48
$16\pi^2\Delta\alpha_5$	σ^+	3.05	2.69	1.17	3.94	1.14
	σ^-	-7.10	-6.40	-2.19	-3.53	-1.64

around the nominal mass. Finally, we take the combination that minimizes the deviation from the PDG values and do a kinematical fit of the bosonic momenta to the total energy and momentum. For a binned likelihood fit, we do not consider the bosonic spins, and choose as observables two invariant masses, $M^2_{WZ} = (p_W + p_Z)^2$, $M^2_{WW} = (p_{W^+} + p_{W^-})^2$, and the angle θ between the e^- beam axis and the direction of the Z-boson.

Results are shown in Fig. 11.3 and Tab. 11.3. For WWZ we give in Fig. 11.3A the 90% contours for the different polarization cases A, B, and C, and for both beams polarized also the 68% contour. The respective $\Delta\alpha_i$ are given in Tab. 11.3. We find that the sensitivity strongly increases with polarization, cf. the different cases A, B, and C. A best combined fit for triple boson production is given in Fig. 11.3B.

11.2.2 Analysis of weak-boson scattering

In this section we consider those six-fermion processes in e^+e^- and e^-e^- collisions that depend on quartic gauge couplings via quasi-elastic weak-boson scattering subprocesses, i.e., $VV \to VV$, where $V = W^\pm, Z$. We use full six-fermion matrix elements and thus do not rely on simplifications such as the effective W approximation, the Goldstone-boson equivalence theorem, or the narrow-width approximation for vector bosons.

For the simulation we assume a c.m. energy of $1\ \mathrm{TeV}$ and a total luminosity of $1000\ \mathrm{fb}^{-1}$ in the e^+e^- mode. Beam polarization of 80% for electrons and 40% for positrons is also assumed. Since the six-fermion processes under consideration contain contributions from triple weak-boson production processes (ZZ or W^+W^- with neutrinos of second and third generation as well as a part of $\nu_e\bar{\nu}_e WW(ZZ)$, $e\nu_e WZ$ and $e^+e^-W^+W^-$ final states), there is no distinct separation of signal and background.

The present study extends the previous study [50] which considered a restricted set of channels and parameters. In addition to the backgrounds considered there, we include single weak-boson production in the background simulation for completeness. We take initial-state radiation into account when generating events. For the generation of $t\bar{t}$ events we use `PYTHIA` [93]. The event samples are generated by the multi-purpose event generator `O'Mega/WHIZARD` [92, 94–96], using exact six-fermion tree-level matrix elements. Hadronization is done with `PYTHIA`. We use the `SIMDET` [97] program to produce the detector response of a possible ILC detector.

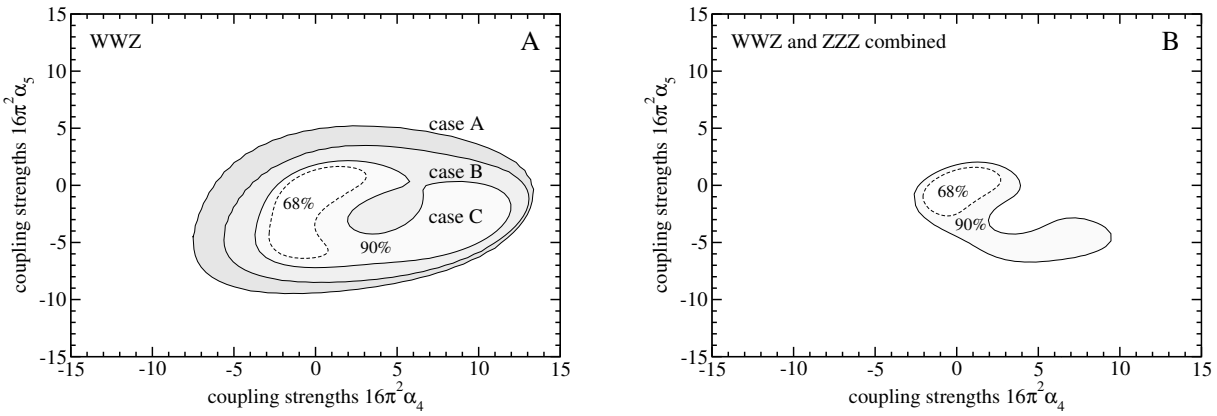

Fig. 11.3: Expected sensitivity for α_4/α_6 and α_5/α_7 at $\sqrt{s} = 1000\,\text{GeV}$. Luminosity assumption $1000\ \text{fb}^{-1}$. A) WWZ-channel only, for an unpolarized beam (A) and the different polarizations cases, e^- only polarized (B) and both beams polarized (C) as explained in the text. Solid lines represent 90% confidence level, the dashed line is for 68%, i.e. $\Delta\chi^2 = 2.3$. B) Combined fit using WWZ of case C and ZZZ production. Lines represent 90% (outer line), 68% (inner line) confidence level.

Table 11.4 contains a summary of all generated processes used for analysis and their corresponding cross sections. For pure background processes a full $1\ \text{ab}^{-1}$ sample is generated. All signal processes are generated with higher statistics. Single weak-boson processes and $q\bar{q}$ events are generated with an additional cut on $M(q\bar{q}) > 130\ \text{GeV}$ to reduce the number of generated events.

The event selection is done by a cut-based approach, using again hadronic W/Z decays. The observables sensitive to the quartic couplings are the total cross section (either reduction or increase depending on the interference term in the amplitude and the point in parameter space), and modification of the differential distributions in vector-boson production angle and decay angle. The extraction of quartic gauge couplings from reconstructed kinematic variables is done by a binned likelihood fit. To determine the dependence of the cross section on the parameters within each bin, starting from an unweighted event sample as generated by `WHIZARD`, we use the complete matrix elements encoded in the event generator itself to reweight each event as a function of the quartic gauge couplings. The obtained four-dimensional event distributions are fitted with `MINUIT` [98], maximizing the likelihood as a function of α_i,α_j.

11.2.3 Combined results and resonance interpretation

In Tables 11.5 and 11.6 we combine our results for the measurement of anomalous electroweak couplings for an integrated luminosity of $1000\ \text{fb}^{-1}$ in the e^+e^- mode, assuming conservation of the custodial symmetry (i.e., $\alpha_{6,7,10} = 0$) and non-conservation, respectively. In Fig. 11.4, the results are displayed in graphical form, projecting the multi-dimensional exclusion region in α space around the reference point $\alpha_i \equiv 0$ onto the two-dimensional subspaces (α_4, α_5) and (α_6, α_7).

In order to get a more intuitive physical interpretation in terms of a new-physics scale, we can transform anomalous couplings into resonance parameters. In each spin/isospin channel we may place a single resonance, one at a time. For each measured value of some α parameter, we may deduce the properties of the resonance that would result in this particular value, assuming that no other contributions to the anomalous couplings are present. Inserting the values that correspond to the sensitivity bound obtained by the experimental analysis, we get a clear picture on the possible sensitivity to resonance-like new physics in the high-energy region.

A resonance in a given scattering channel has two parameters, the mass M and the coupling to this channel. If we are just interested in the sensitivity reach, we have to get rid of the arbitrariness in the coupling. To this end, we first note that the total resonance width does not exceed the mass —

Table 11.4: Generated processes and cross sections for signal and background for $\sqrt{s} = 1$ TeV, polarization 80% left for electron and 40% right for positron beam. For each process, those final-state flavor combinations are included that correspond to the indicated signal or background subprocess.

Process	Subprocess	σ [fb]
$e^+e^- \to \nu_e\bar{\nu}_e q\bar{q}q\bar{q}$	$W^+W^- \to W^+W^-$	23.19
$e^+e^- \to \nu_e\bar{\nu}_e q\bar{q}q\bar{q}$	$W^+W^- \to ZZ$	7.624
$e^+e^- \to \nu\bar{\nu}q\bar{q}q\bar{q}$	$V \to VVV$	9.344
$e^+e^- \to \nu e q\bar{q}q\bar{q}$	$WZ \to WZ$	132.3
$e^+e^- \to e^+e^- q\bar{q}q\bar{q}$	$ZZ \to ZZ$	2.09
$e^+e^- \to e^+e^- q\bar{q}q\bar{q}$	$ZZ \to W^+W^-$	414.
$e^+e^- \to b\bar{b}X$	$e^+e^- \to t\bar{t}$	331.768
$e^+e^- \to q\bar{q}q\bar{q}$	$e^+e^- \to W^+W^-$	3560.108
$e^+e^- \to q\bar{q}q\bar{q}$	$e^+e^- \to ZZ$	173.221
$e^+e^- \to e\nu q\bar{q}$	$e^+e^- \to e\nu W$	279.588
$e^+e^- \to e^+e^- q\bar{q}$	$e^+e^- \to e^+e^- Z$	134.935
$e^+e^- \to X$	$e^+e^- \to q\bar{q}$	1637.405

Table 11.5: The expected sensitivity from 1000 fb$^{-1}e^+e^-$ sample at 1 TeV in the $SU(2)_c$ conserving case, positive and negative one sigma errors given separately.

coupling	$\sigma-$	$\sigma+$
$16\pi^2\alpha_4$	-1.41	1.38
$16\pi^2\alpha_5$	-1.16	1.09

Table 11.6: The expected sensitivity from 1000 fb$^{-1}e^+e^-$ sample at 1 TeV in the broken $SU(2)_c$ case, positive and negative 1 sigma errors given separately.

coupling	$\sigma-$	$\sigma+$
$16\pi^2\alpha_4$	-2.72	2.37
$16\pi^2\alpha_5$	-2.46	2.35
$16\pi^2\alpha_6$	-3.93	5.53
$16\pi^2\alpha_7$	-3.22	3.31
$16\pi^2\alpha_{10}$	-5.55	4.55

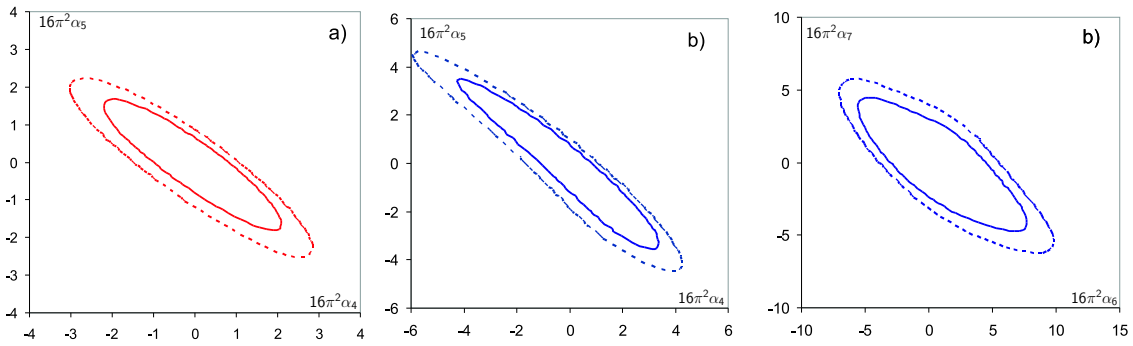

Fig. 11.4: Expected sensitivity (combined fit for all sensitive processes) to quartic anomalous couplings for a 1000 fb^{-1} e^+e^- sample. The full line (inner one) represents 68%, the dotted (outer) one 90% confidence level. a) conserved $SU(2)_c$ case b) broken $SU(2)_c$ case.

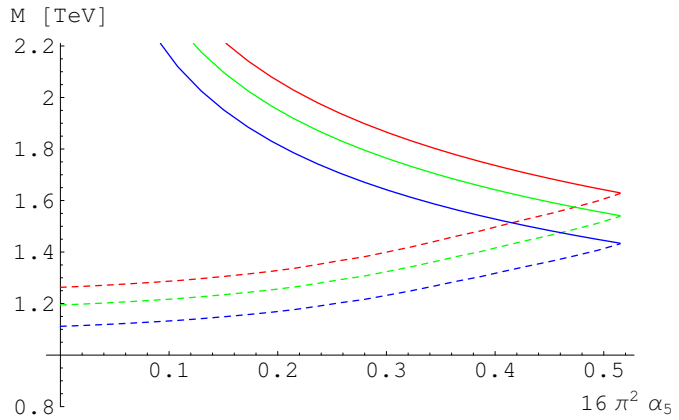

Fig. 11.5: Allowed region for a scalar singlet resonance with isospin breaking as a function of α_5 between the upper (full) and lower bound (dashed). Ratio of width to mass of the resonance equal to 1.0 (top curve, red), 0.8 (middle curve, green), and 0.6 (lower curve, blue), respectively.

Table 11.7: Mass reach for the scalar singlet resonance in the case of isospin breaking.

$f_\sigma = \frac{\Gamma_\sigma}{M_\sigma}$	1.0	0.8	0.6
M_σ [TeV]	1.39	1.32	1.23

otherwise the notion of a resonance is meaningless. To be more specific, we can introduce the ratio of width and mass as a parameter $f \equiv \Gamma/M$. Since the low-energy effect of tree-level resonance exchange is proportional to f^2, the ultimate sensitivity of a low-energy measurement can be associated with the possible maximum $f \approx 1$, i.e., a resonance that is as wide as heavy.

As an example, in Fig. 11.5 we display the allowed mass range for an isosinglet scalar resonance as a function of the measured anomalous coupling α_5, assuming no other new physics to be present. Inserting the sensitivity on α_5 as obtained from the ILC analysis above, we end up with a mass reach, depending on the resonance width ratio, as listed in Table 11.7.

Similar analyses can be carried out for all possible spin/isospin channels, where for the particular case of vector resonances the results from oblique corrections and triple gauge couplings have to be included in the fit. Detailed results can be found in Ref. [51]. Here, we just quote the final results in Table 11.8.

To conclude, from purely bosonic interactions we find limits for the sensitivity of the ILC in the 1 to 3 TeV range, where the best reach corresponds to the highest-spin channel. These limits are not as striking as possible limits from contact interactions, but agree well with the expected direct-search limits for resonances at the LHC. Note that the selection of purely bosonic interaction depends on the choice of operator basis. In concrete models such as the Technicolor, in a generic basis fermionic couplings of new resonances have to be accounted for (cf. the discussion in [51]), and by including those, better limits can be obtained. Our results thus correspond to the 'worst-case' parameter set where new-physics contributions are minimized.

Performing global fits of all electroweak parameters, analogous to LEP analyses, and combining data from both colliders will be important for disentangling the contributions. Significant knowledge about the mechanism of electroweak symmetry breaking can thus be gained even in scenarios that do not lead to striking new-physics signatures at all.

Table 11.8: Accessible resonance mass in TeV for all possible spin/isospin channels. The results are derived from the analysis of vector-boson scattering processes at the ILC, assuming a single resonance with optimal properties. Left: custodial $SU(2)$ symmetry is assumed to hold; right: no constraints beyond the SM symmetries are assumed.

Spin	$I=0$	$I=1$	$I=2$
0	1.55	–	1.95
1	–	2.49	–
2	3.29	–	4.30

Spin	$I=0$	$I=1$	$I=2$
0	1.39	1.55	1.95
1	1.74	2.67	–
2	3.00	3.01	5.84

11.3 WW scattering at high WW centre-of-mass energy

Jonathan M. Butterworth

Given the issues already discussed in the introduction, it is clear that whatever scenario for electroweak symmetry breaking is realised in nature, the measurement of the vector-boson scattering process $qq \to qqWW \to qqWW$, where "W" implies both charged and neutral vector bosons, is a priority for the LHC experiments. Without a Higgs, the standard model makes no prediction for this cross section above 1.2 TeV; put another way - this cross section is almost entirely determined by the electroweak symmetry-breaking mechanism, and thus is the most model-independent probe of this mechanism.

These processes have been widely studied (see references in the previous section). However, many of these processes focus on Higgs searching. In this case, the mass range of interest is well below 1 TeV, and in addition, since one is searching for a resonance, it is acceptable to look for threshold enhancements in a lepton transverse momentum spectrum where both W's decay leptonically. However, since the cross section is dominated by charged vector bosons, this implies the presence of two neutrinos in the final state, and prohibits an accurate measurement of the WW centre-of-mass energy.

Here we briefly summarise a study [33] of the charged-WW scattering process at WW centre-of-mass energies of 0.6 TeV and above. This study was motivated by the desire to measure the WW cross section as a function of WW centre-of-mass energy as accurately as possible, regardless of the (unknown) structure of the cross section. Therefore the requirement of sufficient statistics at the extreme kinematic limit, as well as the requirement that a maximum of one neutrino be in the final state, and the control of QCD backgrounds, drives the study toward measuring the cross section where one W decays leptonically and the other decays hadronically.

The high energy implies that the decaying W's are very highly boosted. This aids reconstruction of the neutrino kinematics, but implies that the hadronically decaying W is generally reconstructed as a single jet. The principal backgrounds are W+jet production where the jet fakes a hadronic W, and $t\bar{t}$ production.

One interesting feature of the study was the use of the k_T jet algorithm [99] to reconstruct the jets. This is theoretically preferred to simple cone algorithms, meaning that comparisons to predictions can eventually be made with greater confidence. This is in part because it mirrors the structure of the QCD cascade itself. This property can be exploited in identifying the hadronically-decaying W, since in this case the highest k_T "splitting" of the jet is expected to be the W decay, i.e. at a characteristic scale of M_W, whereas for the QCD jet in the W+jet process, it is a gluon radiation which will typically be at a scale much lower than the p_T of the jet. By decomposing the W-candidate jet into subjets in the k_T algorithm, this splitting scale may be evaluated and used to suppress the W+jet background. This is similar in principle to rerunning the cone algorithm with a smaller cone, as was done in previous studies; however, the k_T approach is better theoretically controlled, less ambiguous and is invariant under boosts along the W direction. The latter property is particularly important when the desire is to study the shape of the cross section as a function of the WW centre-of-mass energy. This technique is in fact generally

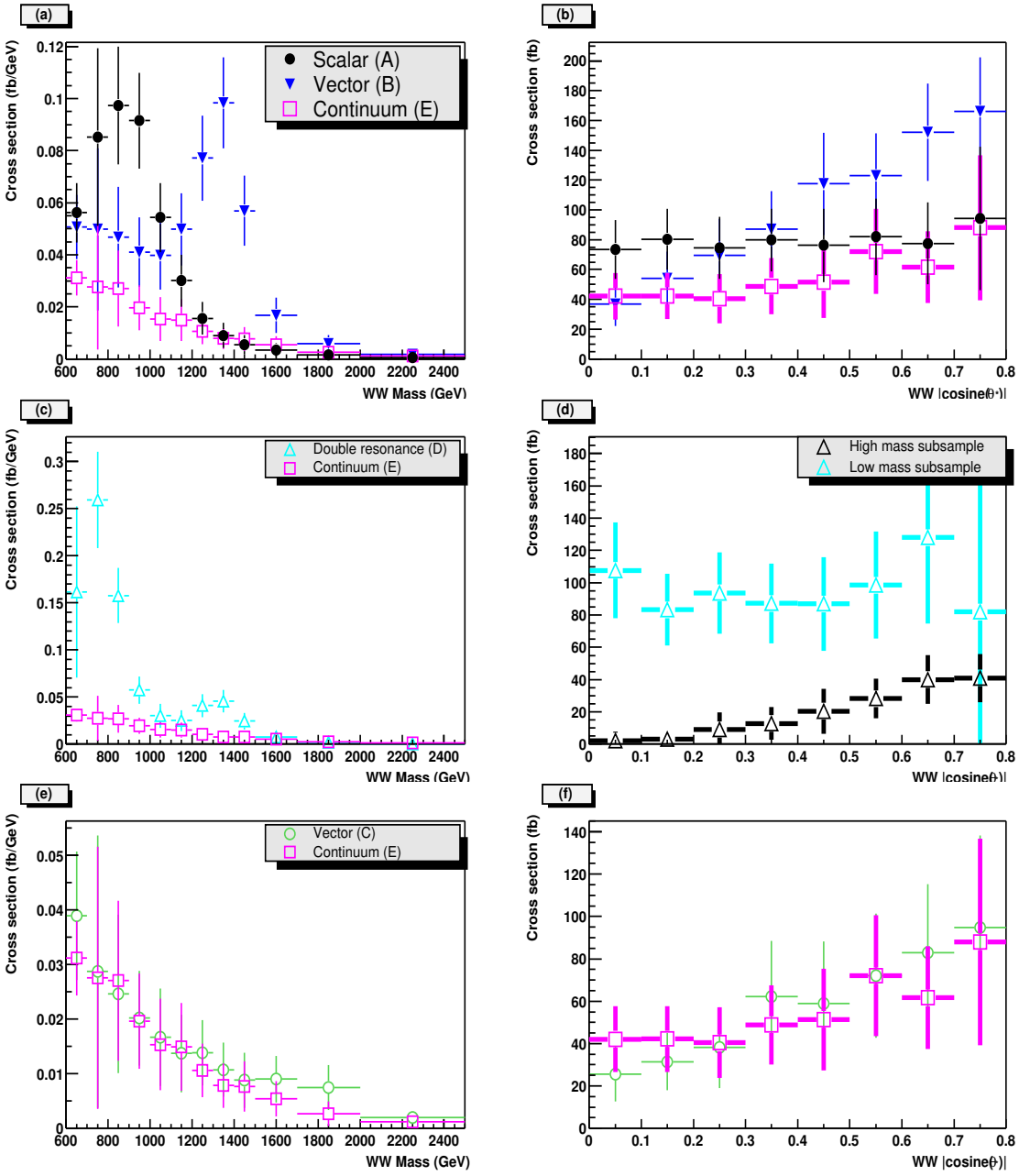

Fig. 11.6: Measurement expectation after 100 fb^{-1} of LHC luminosity at 14 TeV cm energy. (a,c,e) $d\sigma/dM_{WW}$ and (b,d,f) $d\sigma/d|\cos\theta^*|$. (d) shows $d\sigma/d|\cos\theta^*|$ for the high and low mass subsamples for the double resonance model, separated by a cut at 1200 GeV. (Figure taken from [33]).

applicable to any highly boosted massive particle decaying to hadrons. We note that the k_T algorithm is available in a standard implementation, used by the experiments and theorists alike [100], and a recent reimplementation improves the speed dramatically [101], a factor which was previously a limitation on its use.

Other new features of the analysis included a top quark veto and a cut on the transverse momentum of the hard subsystem. In addition, the established tag jet and minijet veto cuts were applied.

Five different physics scenarios, representative of the different types of physics which might reasonably be expected at the LHC, were studied. The effect of uncertainties in the underlying event leads to a model dependent systematic error of 40-50%. The results compare very well with previous Higgs

search studies in the semi-leptonic channel. Over a wide range of parameter space signal/background ratios of greater than unity can be obtained, and the cross-section can be measured differentially in the WW centre-of-mass energy within one year of high luminosity LHC running (100 fb^{-1}). Vector and scalar resonances up to around 1.5 TeV may well be observable, and their spins measureable. Figure 11.6 shows the simulated measurements, after background subtraction, estimated for 100 fb^{-1} of LHC luminosity at 14 TeV cm energy.

These studies are currently being repeated and updated using a simulation of the ATLAS detector [102–104]. Early indications are that the conclusions are robust against detector effects, but clearly much more detailed work is needed to realise these measurements in LHC data.

11.4 VV-fusion in CMS: a model-independent way to investigate EWSB

Elena Accomando, Nicola Amapane, Alessandro Ballestrero, Aissa Belhouari, Riccardo Bellan, Giuseppe Bevilacqua, Sara Bolognesi, Gianluca Cerminara, Vladimir Kashkan, Ezio Maina and Chiara Mariotti

Vector boson scattering is the reaction of choice to probe the nature of Electroweak Symmetry Breaking (EWSB), for which the Standard Model (SM) provides the simplest and most economical explanation. In the SM the Higgs particle is essential to the renormalizability of the theory and is also crucial to ensure that perturbative unitarity bounds are not violated in high energy reactions. Scattering processes between longitudinally polarized on shell vector bosons (V_L) are particularly sensitive in this regard. Without a Higgs the V_L's interact strongly at high energy, violating perturbative unitarity at about one TeV. If, on the contrary, a relatively light Higgs exists then they are weakly coupled [105]. In the strong scattering case one is led to expect the presence of resonances in V_LV_L interactions. Unfortunately the mass, spin and even number of these resonances are not uniquely determined [33]. If a Higgs particle is discovered it will nonetheless be necessary to verify that indeed longitudinally polarized vector bosons are weakly coupled at high energy by studying boson boson scattering in full detail. Studying the large mass region of boson-boson scattering could provide an alternative method to determine the Higgs mass range. This could be very useful in case of a light Higgs which will require several years of data taking for a reliable discovery.

In the absence of firm predictions in the strong scattering regime, trying to gauge the possibilities of discovering signals of new physics at the LHC requires the somewhat arbitrary definition of a model of V_LV_L scattering beyond the boundaries of the SM. The simplest approach is to consider the SM in the presence of a very heavy Higgs. While this entails the violation of perturbative unitarity, the linear rise of the cross section with the invariant mass squared in the hard VV scattering will be swamped by the decrease of the parton luminosities at large momentum fractions and, as a consequence, will be particularly challenging to detect. At the LHC, the offshellness of the incoming vector bosons will further increase the difference between the expectations based on the behaviour of on shell VV scattering and the actual results. For M_H >10 TeV, all Born diagrams with Higgs propagators become completely negligible in the Unitary gauge, and all expectations reduce to those in the $M_H \to \infty$ limit. Since this limit is gauge invariant, the results for the no Higgs case presented in the following do not depend on the gauge choice.

At the LHC no beam of on shell EW bosons will be available. Incoming quarks will emit spacelike virtual bosons which will then scatter among themselves and finally decay. All previous studies of boson boson scattering at high energy hadron colliders, with the exception of Refs. [64, 106], have resorted to some approximation, either the Equivalent Vector Boson Approximation (EVBA), or a production times decay approach. There are however issues that cannot be tackled without a full six fermion calculation like exact spin correlations between the decays of different heavy particles, the effect of the non resonant background, the relevance of the offshellness of boson decays, the question of interferences between different subamplitudes.

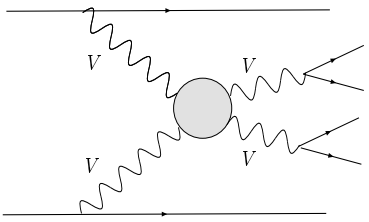

Fig. 11.7: The general diagram of vector boson fusion processes.

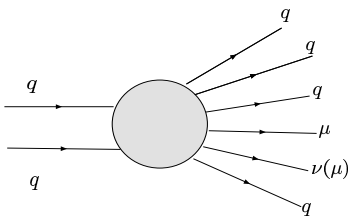

Fig. 11.8: The $qq \to qqqq\mu\nu/\mu$ process generic diagram.

11.4.1 Semileptonic final states

At the LHC the large VV invariant mass region can be explored studying the following processes

$$qq \to qqVW \to qqqq\mu\nu$$
$$qq \to qqVZ \to qqqq\mu\mu$$

They offer a clear experimental signature, because of the presence of high p_T muons from the W or Z decay, together with the highest branching ratio among the final states which can be reconstructed in an hadronic environment. In fact boson boson scattering with a totally hadronic final state cannot be isolated from the non resonant QCD background whose cross section is much larger while final states where both bosons decay leptonically have a smaller rate. Moreover in $qqWW \to qq\mu\nu\mu\nu$ processes the VV invariant mass cannot be reconstructed. Up to now, only final states with muons have been considered, but processes with electrons can be used as well. In the future four lepton final state channels will also be studied.

11.4.2 Signal definition and simulation

In order to explore the EWSB mechanism through the analysis of VV scattering processes, a precise knowledge of the cross section $\sigma(qq \to qqVV)$ over the whole VV invariant mass spectrum is essential. The choice of the MC generator is therefore a key aspect of this study. The $qq \to qqqq\mu\nu$ processes have been simulated with `PHASE` [107, 108] and the $qq \to qqqq\mu\mu$ with `PHANTOM` which are exact leading order matrix element MC's at order α^6_{EW}.

The general diagram of the vector boson fusion process is shown in Fig. 11.7. Once vector bosons are decayed we have a six fermion final state. If the virtuality of the incoming vector bosons is properly taken into account and the outgoing vector bosons are allowed to be off mass shell then the full set of diagrams describing $qq \to qqqqll'$ has to be considered in order to preserve gauge invariance (see Fig. 11.8). This process includes not only boson boson scattering but also all the irreducible backgrounds that interfere with the signal and cannot be computed and simulated separately. They include the production of a VV pair produced without undergoing scattering as well as diagrams describing $t\bar{t}$ and single top electroweak production. Furthermore there can be subprocesses with three outgoing vector bosons from Triple or Quartic Gauge Couplings or from Higgs production via Higgstrahlung. Finally "non resonant"

Table 11.9: Standard acceptance cuts applied during event simulation. Here lepton refers only to $l^{\pm}$.

E(quarks)$>$ 20 GeV	E(lepton)$>$ 20 GeV
p_T(quarks)$>$ 10 GeV	p_T(lepton)$>$ 10 GeV
$\|\eta$(quarks)$\| < 6.5$	$\|\eta$(lepton)$\| < 3$
M(qq)$>$ 20 GeV	M(ll)$>$ 20 GeV

Table 11.10: Cross sections and percentages of $qq \to 4q\mu\nu$ and $qq \to 4q\mu\mu$ events generated for the signal and the irreducible background.

	$qq \to qqqq\mu\nu$				$qq \to qqqq\mu\mu$			
	no Higgs		500 GeV		no Higgs		500 GeV	
	σ (pb)	perc.	σ (pb)	perc.	σ (pb)	perc.	σ (pb)	perc.
total	0.689	100%	0.718	100%	0.0430	100%	0.0482	100%
signal	0.158	23%	0.184	26%	0.0170	39%	0.0213	44%
top	0.495	72%	0.494	69%	0.0206	48%	0.0206	43%
non resonant	0.020	3%	0.023	3%	0.0039	9%	0.0046	10%
three bosons	0.016	2%	0.017	2%	0.0015	4%	0.0017	3%

diagrams are considered where only one pair of fermions in the final state comes from a vector boson decay. For a detailed description of all these contributions see [64].

11.4.2.1 $qqVV$ signal selection at partonic level

In order to comply with the acceptance of the CMS detector and with the CMS trigger requirements, the cuts shown in Table 11.9 have been applied to all events.

With the aim to enhance the contribution of boson boson scattering with respect to the irreducible background and investigate EWSB, additional kinematical cuts have been applied at parton level. Single top and $t\bar{t}$ production are the main backgrounds. They represent about 70% (45%) of the total cross section in the $4q\mu\nu$ ($4q\mu^{+}\mu^{-}$) channel. To suppress them, events with a b-quark and two other quarks (with flavour compatible with W decay) are rejected if the invariant mass of these three particles is between 160 and 190 GeV. Analogously, events in which the muon, the neutrino and a b-quark have an invariant mass between 160 and 190 GeV are rejected.

The two leptons have to reconstruct the mass of a W or a Z, so their invariant mass is required to be in the range $M_V \pm 10$ GeV. In VV fusion an additional W or a Z decaying hadronically is expected to be present. Therefore events are required to contain two quarks with the correct flavours to be produced in W or Z decay and with an invariant mass of $\pm$ 10 GeV around the central value of the corresponding gauge boson. If more than one combination of two quarks satisfy these requirements, the one closest to the corresponding central mass value is selected. This combination will in the following be assumed to originate from the decay of an EW vector boson. The requirement of at least two reconstructed vector bosons in the final state eliminates about 3% (10%) of the total cross section. Finally one has to reject events with the production of three outgoing vector bosons: if the two remaining quarks have the right flavour to reconstruct a W or a Z boson and if their invariant mass is compatible within 10 GeV with the corresponding boson mass then the event is rejected. This happens in about 2% (3%) of the cases. As shown in [106] the requirement that quark pairs which have masses in the neighborhood of the EW vector boson masses also have the correct flavour content has a very modest impact on our results.

In the following we will refer as "signal" to the events which pass the selection cuts in Table 11.9 and the additional kinematical cuts mentioned above: top veto and presence of two and only two particle

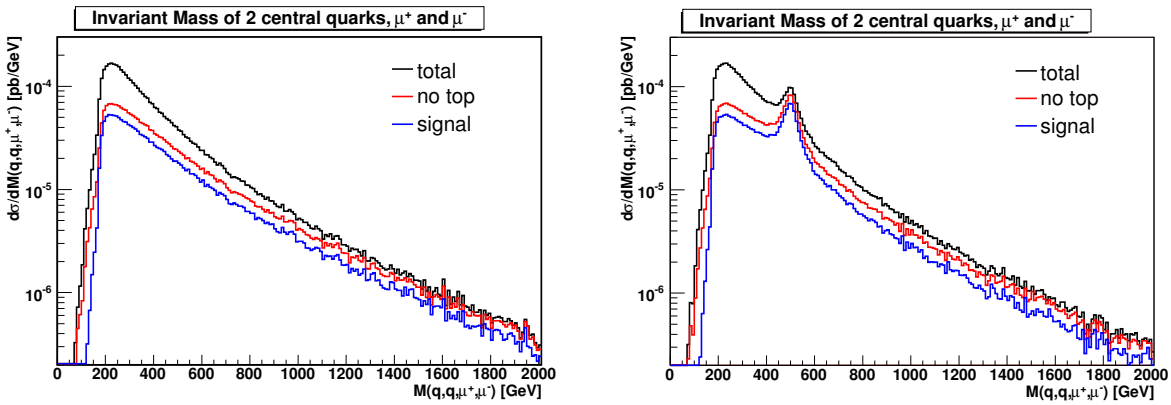

Fig. 11.9: Distributions of the invariant mass of the two central quarks, the muon and the neutrino for the no-Higgs case (left). Distributions of the invariant mass of the two central quarks and the two muons for M(H)=500 GeV (right). The top curve refers to the full sample. The intermediate one shows the effects of antitagging on the top. The lowest line corresponds to imposing all the mentioned cuts and antitagging on the presence of three vector bosons.

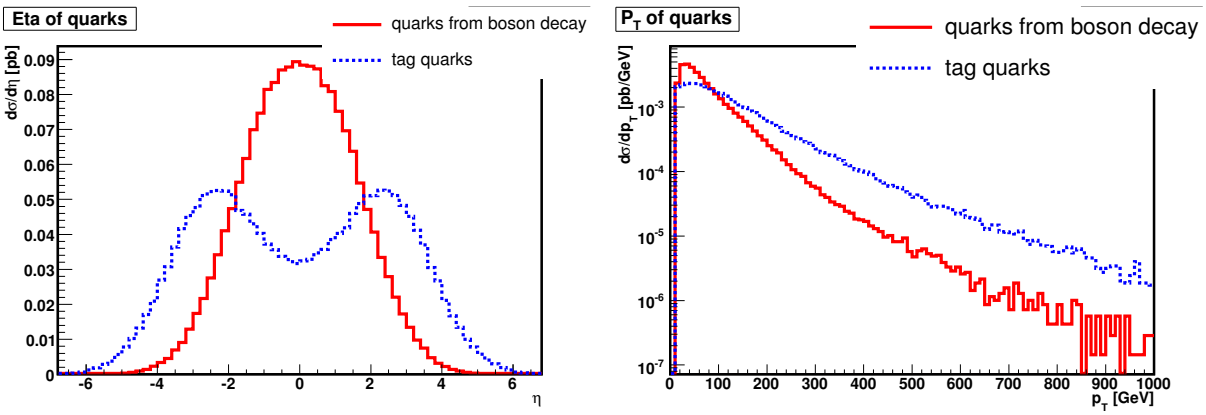

Fig. 11.10: Pseudorapidity and transverse momentum of the two quarks from the boson decay and of the two tag quarks in the no-Higgs scenario for the $4q\mu\nu$ channel.

pairs (ll and jj) with masses close to the masses of the EW vector bosons. In Table 11.10 we list the cross sections for the signal and the irreducible backgrounds corresponding to the described cuts. In Fig. 11.9, the M(VW) spectrum is shown.

11.4.2.2 Signal topology

The lepton and the neutrino (l^+l^- pair) in the final state come from the decay of a W (Z). They are expected to have a quite high transverse momentum (p_T) and to be mostly produced centrally in the detector, i.e. at low absolute value of the pseudo-rapidity (η). Similarly the two quarks from the decay of the second vector boson. On the contrary, the two quarks which emit the two incoming vector bosons tend to go in the forward/backward region (high $|\eta|$) with very large energy and p_T. Thanks to their peculiar kinematical pattern these two spectator quarks are essential to tag the VV fusion events among all six fermions final states, therefore they will also be called "tag quarks". In Fig. 11.10 the kinematics of the two quarks from the boson decay and of the two tag quarks are compared.

It is interesting to look at possible differences in the kinematics of the VV-fusion signal with respect to the irreducible background. In Fig. 11.11 the distributions of some kinematical variables are presented for the signal and for the full sample in case of the $qqqq\mu\nu$ final state. We expect similar

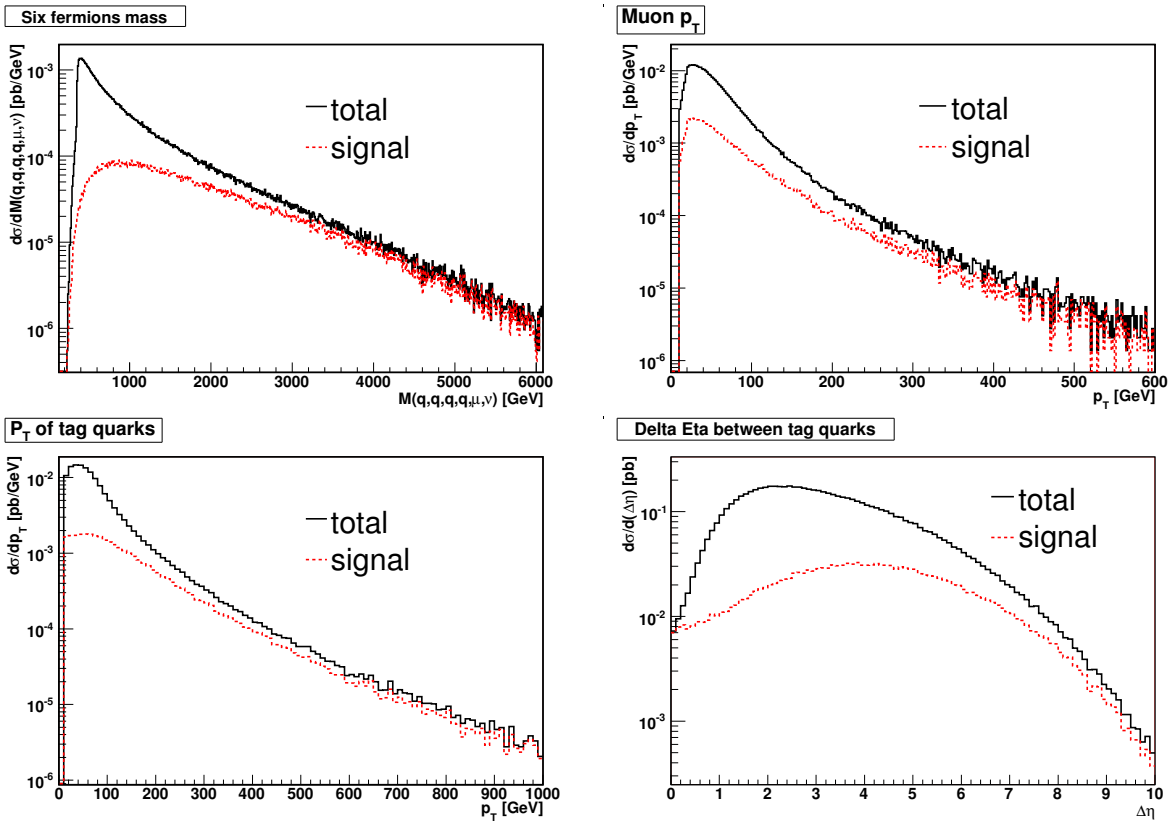

Fig. 11.11: Differential cross section in the $4q\mu\nu$ case as a function of the invariant mass of the six fermions in the final state, the transverse momentum of the muon, the transverse momentum of the two tag quarks, and the difference in pseudorapidity between the two tag quarks for all the events (black) and for the signal events (red). All plots refer to the no-Higgs case.

results for the $qqqq\mu^+\mu^-$ final state as well. In the figure the no-Higgs case is chosen as an example, but there are no significant differences with the case of a visible Higgs. Only some variables, which are connected to the mass of the Higgs boson, show the presence of the resonance. The total invariant mass of the six fermions in the final state is presented for the signal and for the full sample: the signal tends to have a very large final six fermion mass. The muon from the signal has a larger p_T than the one from the background, and the same applies to the spectator quarks. The difference of the η's of the tag quarks is also shown: the signal tends to have a larger $\Delta\eta$ with respect to the background.

11.4.2.3 Main backgrounds

The most problematic background for the vector boson fusion signal is the production of a single W (or Z) in association with n jets (n=1,2,3,4). In this case the outgoing jets come from gluons or quarks produced via QCD processes, so we expect a larger occupancy of the central pseudorapidity region with respect to the pure EW signal process.

$t\bar{t}$ and single top production via QCD processes, e.g. $q\bar{q} \rightarrow t\bar{t}$ and $gg \rightarrow t\bar{t}$, are other backgrounds with very large cross sections. Top quarks decay into a W boson and a b-quark with a branching ratio of almost 100% giving a final state similar to that produced in VV fusion events. However the outgoing b-quarks can be recognized through a b-tagging algorithm and they have a kinematical behaviour quite different from the signal tag quarks: the former are in fact more central and have much lower energy.

Exactly the same final state of the signal $jjVW \rightarrow jjqq\mu\nu$ (or $jjVZ \rightarrow jjqq\mu\mu$) can be pro-

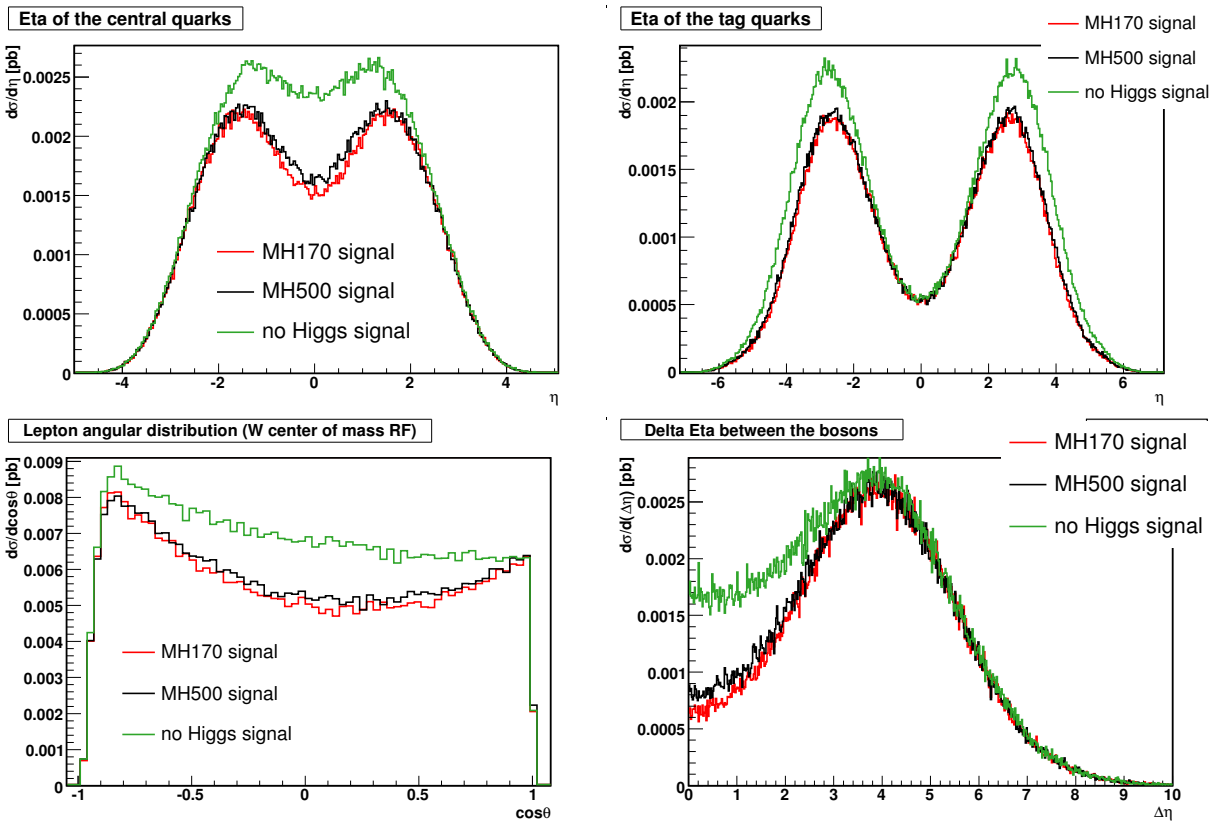

Fig. 11.12: The pseudorapidity η of the two central jets, the η of the forward quarks, the cosine of the angle between the lepton and the W boson in the W boson rest frame and the $\Delta\eta$ of the two vector bosons for $M(VW) > 800$ GeV in the $4q\mu\nu$ channel. In green for the no-Higgs case, in black for M(H)=500 GeV and in red for M(H)=170 GeV.

duced also at a different perturbative order: $\alpha_S^2\alpha_{EW}^4$. In this case the two jets not coming from a boson decay are generated from QCD processes so they can come from a quark or a gluon. These background processes can be distinguished from the VV fusion signal thanks to the fact that in the first case the outgoing bosons have very high energy and quite high pseudorapidity so they have lower transverse momentum with respect to the signal bosons that are produced in the central region. Moreover the two outgoing QCD quarks (or gluons) have very high energy, higher than the energy of the signal tag quarks, and their pseudorapidity distribution and their transverse momentum spectrum are intermediate between that of the signal quarks from the boson decay and that of the signal tag quarks.

Some preliminary studies have been done with the CMS detector fast simulation (refs. [109], [110], [111], [112]). In these references you can find a detailed description of all mentioned backgrounds together with some preliminary strategies to eliminate them and to reconstruct the signal in the CMS detector.

11.4.3 The high mass region

An interesting physics possibility is to investigate whether there exist or not an elementary Higgs boson by measuring the VW cross section at large M(VW). The rise of the cross section related to unitarity violation in the no-Higgs case is difficult to detect at the LHC, since the center-of-mass energy is still rather low and the decrease of the proton distribution functions at large x has the dominant effect.

As discussed in [64], the unitarity violation is related only to the scattering of longitudinally polar-

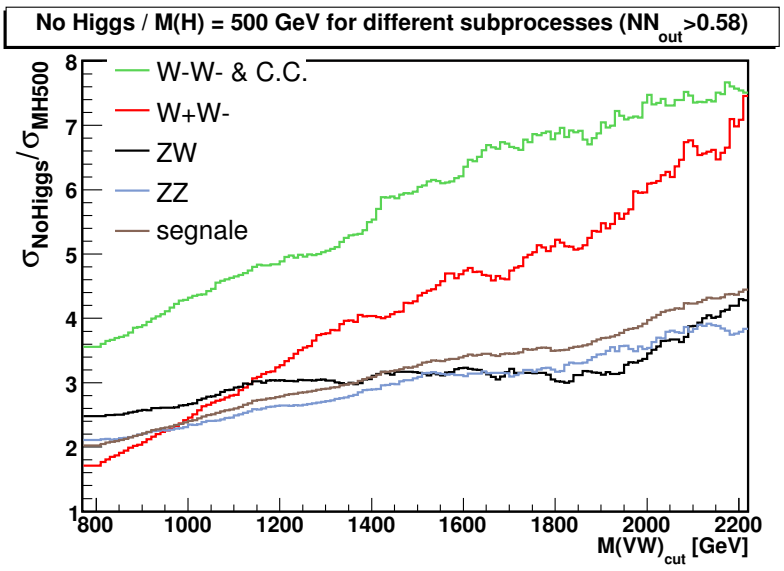

Fig. 11.13: The ratio in Eq.(11.22) for different groups of processes of $4q\mu\nu$ type, for a given cut on NN, the Neural Network output variable.

ized vector bosons. In fact, in presence of a light Higgs, the cross section at high VW invariant masses is due essentially to transversely polarized bosons while in the no Higgs case the cross section the contributions of longitudinally and transversely polarized bosons are comparable. Thus, if it was possible to distinguish W_LW_L from W_TW_T the difference in cross section at high masses between the no Higgs and the light Higgs scenarios would be sizeable. In order to distinguish W_LW_L from W_TW_T we must exploit the different behaviour of the final state in the two cases. Preliminary studies in this direction have been presented in [64].

In Fig. 11.12 several kinematical distributions for M(H)=170 GeV, M(H)=500 GeV and the no-Higgs case have been compared for M(VW)>800 GeV in the $qqqq\mu\nu$ final state[2]. The variables most sensitive to the different behaviour of the two cases (Higgs and no Higgs) have been selected and then used to train a Neural Network focusing on events in the high mass region (M(VV)>800 GeV).

Thus the Neural Network becomes able to distinguish the light Higgs from the no Higgs scenario and a significative difference in the integrated cross section in these two cases can be achieved imposing a cut on the Neural Network output. It is also interesting to study how the difference at high invariant masses changes if we consider different processes. In Fig. 11.13 we show the ratio

$$\frac{\int_{M_{cut}}^{\infty} dM_{VW} \frac{d\sigma_{noHiggs}}{dM_{VW}}}{\int_{M_{cut}}^{\infty} dM_{VW} \frac{d\sigma_{M_H=500}}{dM_{VW}}} \tag{11.22}$$

for different groups of processes for a given cut on the Neural Network output (for details see [64]). The set which includes $W^{\pm}W^{\pm} \to W^{\pm}W^{\pm}$ is the one with the largest separation, while the sets including $ZZ \to W^{\pm}W^{\mp}$ and $ZW \to ZW$ scattering show a smaller difference between the Higgs/no–Higgs scenarios.

For the final states $4q\mu^+\mu^-$ simple kinematical cuts have been applied to enhance the difference between the case of Higgs and no Higgs [106]. With the requirement of $|\eta(V)| < 2$ we obtain a difference

[2]Recall that only purely EW processes has been included in this study.

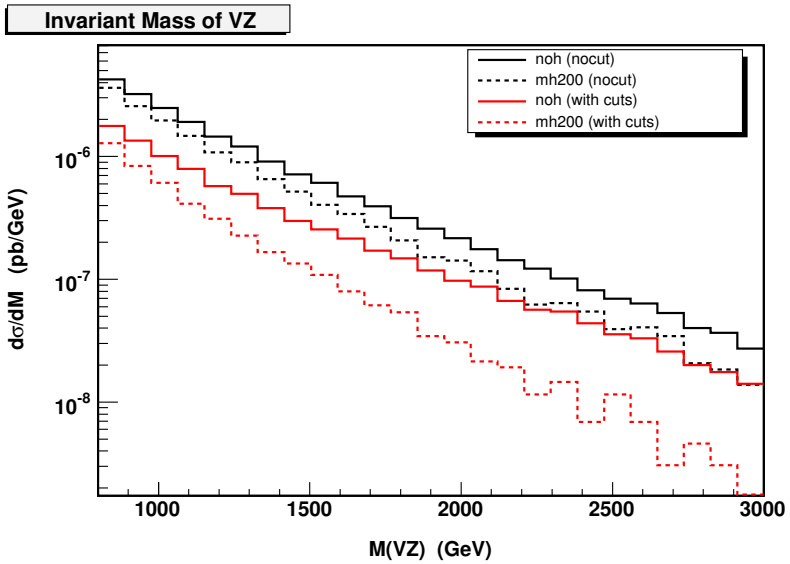

Fig. 11.14: Invariant mass distribution for $M(VZ) > 800$ GeV in the $4q\mu^+\mu^-$ case. The full line refers to the no-Higgs case, the dashed one to M(H)=200 GeV. The upper two curves present the results for our signal definition. For the two lower ones we have further required $|\eta(Z_{ll})| < 2$ and $|\eta(q_V)| < 2$.

between the Higgs/no–Higgs case of a factor 2 to 3 with a cross section of 0.4 to 0.04 in the first case and 0.7 to 0.1 fb in the no Higgs scenario (see Fig. 11.14).

11.4.4 Summary and future

We have studied at parton level the processes $qq \to qqqq\mu\nu$ and $qq \to qqqq\mu\mu$ at the LHC using two new MonteCarlo generators `PHASE` and `PHANTOM`. A strategy to enhance boson boson scattering with respect to the irreducible backgrounds has been developed.

The SM predictions in the absence of the Higgs have been chosen as a benchmark scenario for possible signals of new physics in the EWSB sector: a comparison with the standard case of a visible Higgs has been performed focusing on the high M(VV) region.

The effect of the CMS detector is under study. Preliminary analyses [112], using different generators and an old version of the detector simulation, showed that at CMS a good resolution on the M(VV) variable can be achieved along with a resonable signal over background ratio. Since the cross section of the process is very small a few years of data taking will be necessary to be able to study these channels.

Channels with four leptons in the final state will be investigated in the near future.

REFERENCES

[1] Particle Data Group, S. Eidelman *et al.*, Phys. Lett. **B592**, 1 (2004).

[2] C. P. Burgess and D. London, Phys. Rev. **D48**, 4337 (1993), [hep-ph/9203216].

[3] C. P. Burgess, S. Godfrey, H. Konig, D. London and I. Maksymyk, Phys. Rev. **D49**, 6115 (1994), [hep-ph/9312291].

[4] S. Weinberg, Phys. Rev. **166**, 1568 (1968).

[5] S. R. Coleman, J. Wess and B. Zumino, Phys. Rev. **177**, 2239 (1969).

[6] J. Callan, G. Curtis, S. R. Coleman, J. Wess and B. Zumino, Phys. Rev. **177**, 2247 (1969).

[7] T. Appelquist and C. W. Bernard, Phys. Rev. **D22**, 200 (1980).

[8] A. C. Longhitano, Phys. Rev. **D22**, 1166 (1980).

[9] A. C. Longhitano, Nucl. Phys. **B188**, 118 (1981).

[10] A. Dobado, A. Gomez-Nicola, A. Maroto and J. R. Pelaez, *Effective Lagrangians for the Standard Model* (Springer, New York, 1997).

[11] W. Kilian, *Electroweak Symmetry Breaking: The Bottom-Up Approach* (Springer, New York, 2003).

[12] W. Kilian, hep-ph/0303015.

[13] D. A. Ross and M. J. G. Veltman, Nucl. Phys. **B95**, 135 (1975).

[14] M. J. G. Veltman, Acta Phys. Polon. **B8**, 475 (1977).

[15] M. J. G. Veltman, Nucl. Phys. **B123**, 89 (1977).

[16] P. Sikivie, L. Susskind, M. B. Voloshin and V. I. Zakharov, Nucl. Phys. **B173**, 189 (1980).

[17] J. Gasser and H. Leutwyler, Ann. Phys. **158**, 142 (1984).

[18] J. Gasser and H. Leutwyler, Nucl. Phys. **B250**, 465 (1985).

[19] M. E. Peskin and T. Takeuchi, Phys. Rev. Lett. **65**, 964 (1990).

[20] M. E. Peskin and T. Takeuchi, Phys. Rev. **D46**, 381 (1992).

[21] OPAL Collaboration, The LEP Electroweak Working Group, hep-ex/0511027.

[22] K. J. F. Gaemers and G. J. Gounaris, Z. Phys. **C1**, 259 (1979).

[23] K. Hagiwara, R. D. Peccei, D. Zeppenfeld and K. Hikasa, Nucl. Phys. **B282**, 253 (1987).

[24] M. Dobbs, AIP Conf. Proc. **753**, 181 (2005), [hep-ph/0506174].

[25] S. Hassani, Czech. J. Phys. **54**, A239 (2004).

[26] E. Accomando *et al.* (ECFA/DESY LC Physics Working Group), Phys. Rep. **299**, 1 (1998), [hep-ph/9705442].

[27] J. A. Aguilar-Saavedra *et al.* (ECFA/DESY LC Physics Working Group), hep-ph/0106315.

[28] V. D. Barger, K. Cheung, T. Han and R. J. N. Phillips, Contribution to the Proc. of 1990 Summer Study on High Energy Physics: Research Directions for the Decade, Snowmass, CO, Jun 25–Jul 13, 1990.

[29] J. Bagger *et al.*, Phys. Rev. **D49**, 1246 (1994), [hep-ph/9306256].

[30] J. Bagger *et al.*, Phys. Rev. **D52**, 3878 (1995), [hep-ph/9504426].

[31] O. J. P. Eboli, M. C. Gonzalez-Garcia and J. K. Mizukoshi, Phys. Rev. **D58**, 034008 (1998), [hep-ph/9711499].

[32] A. S. Belyaev *et al.*, Phys. Rev. **D59**, 015022 (1999), [hep-ph/9805229].

[33] J. M. Butterworth, B. E. Cox and J. R. Forshaw, Phys. Rev. **D65**, 096014 (2002), [hep-ph/0201098].

[34] V. D. Barger, K. Cheung, T. Han and R. J. N. Phillips, Phys. Rev. **D52**, 3815 (1995), [hep-ph/9501379].

[35] E. Boos *et al.*, Phys. Rev. **D57**, 1553 (1998), [hep-ph/9708310].

[36] T. Han, H.-J. He and C. P. Yuan, Phys. Lett. **B422**, 294 (1998), [hep-ph/9711429].
[37] E. Boos *et al.*, Phys. Rev. **D61**, 077901 (2000), [hep-ph/9908409].
[38] W. Kilian, Int. J. Mod. Phys. **A15**, 2387 (2000).
[39] F. Larios, T. Tait and C. P. Yuan, Phys. Rev. **D57**, 3106 (1998), [hep-ph/9709316].
[40] T. Han, Y. J. Kim, A. Likhoded and G. Valencia, Nucl. Phys. **B593**, 415 (2001), [hep-ph/0005306].
[41] T. Han, G. Valencia and Y. Wang, Phys. Rev. **D70**, 034002 (2004), [hep-ph/0405055].
[42] B. W. Lee, C. Quigg and H. B. Thacker, Phys. Rev. Lett. **38**, 883 (1977).
[43] B. W. Lee, C. Quigg and H. B. Thacker, Phys. Rev. **D16**, 1519 (1977).
[44] M. S. Chanowitz and M. K. Gaillard, Phys. Lett. **B142**, 85 (1984).
[45] G. L. Kane, W. W. Repko and W. B. Rolnick, Phys. Lett. **B148**, 367 (1984).
[46] S. Dawson, Nucl. Phys. **B249**, 42 (1985).
[47] C. E. Vayonakis, Nuovo Cim. Lett. **17**, 383 (1976).
[48] M. S. Chanowitz and M. K. Gaillard, Nucl. Phys. **B261**, 379 (1985).
[49] G. J. Gounaris, R. Kogerler and H. Neufeld, Phys. Rev. **D34**, 3257 (1986).
[50] R. Chierici, S. Rosati and M. Kobel, Prepared for 5th International Linear Collider Workshop (LCWS 2000), Fermilab, Batavia, Illinois, 24-28 Oct 2000.
[51] M. Beyer *et al.*, hep-ph/0604048.
[52] R. Casalbuoni, S. De Curtis, D. Dominici and R. Gatto, Phys. Lett. **B155**, 95 (1985).
[53] R. Casalbuoni, S. De Curtis, D. Dominici and R. Gatto, Nucl. Phys. **B282**, 235 (1987).
[54] R. Casalbuoni, S. De Curtis and D. Dominici, Phys. Lett. **B403**, 86 (1997), [hep-ph/9702357].
[55] S. N. Gupta, *Quantum Electrodynamics* (Gordon and Breach, New York, 1977).
[56] M. S. Chanowitz, Phys. Rep. **320**, 139 (1999), [hep-ph/9903522].
[57] A. Dobado and J. R. Pelaez, Phys. Rev. **D56**, 3057 (1997), [hep-ph/9604416].
[58] A. Dobado, M. J. Herrero, J. R. Pelaez and E. Ruiz Morales, Phys. Rev. **D62**, 055011 (2000), [hep-ph/9912224].
[59] A. Gomez Nicola and J. R. Pelaez, Phys. Rev. **D65**, 054009 (2002), [hep-ph/0109056].
[60] A. Myagkov, ATLAS note: ATL-PHYS-99-006.
[61] G. Azuelos, R. Mazini and A. Myagkov, ATLAS note: ATL-PHYS-99-006.
[62] F. Gianotti *et al.*, Eur. Phys. J. **C39**, 293 (2005), [hep-ph/0204087].
[63] E. Accomando, A. Ballestrero, A. Belhouari and E. Maina, hep-ph/0505225.
[64] E. Accomando, A. Ballestrero, S. Bolognesi, E. Maina and C. Mariotti, hep-ph/0512219.
[65] R. Casalbuoni *et al.*, Phys. Lett. **B349**, 533 (1995), [hep-ph/9502247].
[66] R. Casalbuoni *et al.*, Phys. Rev. **D53**, 5201 (1996), [hep-ph/9510431].
[67] T. Appelquist and F. Sannino, Phys. Rev. **D59**, 067702 (1999), [hep-ph/9806409].
[68] T. Appelquist, P. S. Rodrigues da Silva and F. Sannino, Phys. Rev. **D60**, 116007 (1999), [hep-ph/9906555].
[69] R. Casalbuoni, S. De Curtis and M. Redi, Eur. Phys. J. **C18**, 65 (2000), [hep-ph/0007097].
[70] D. Dominici, Proc. Snowmass 2001, Snowmass Village, CO, 2001, eConf **C010630**, P329 (2001), [hep-ph/0110084].
[71] A. Caner and M. A. Spezziga, CMS note 2000/072.
[72] C. J. C. Burges and H. J. Schnitzer, Nucl. Phys. **B228**, 464 (1983).
[73] C. N. Leung, S. T. Love and S. Rao, Z. Phys. **C31**, 433 (1986).
[74] W. Buchmuller and D. Wyler, Nucl. Phys. **B268**, 621 (1986).
[75] A. De Rujula, M. B. Gavela, P. Hernandez and E. Masso, Nucl. Phys. **B384**, 3 (1992).

[76] K. Hagiwara, S. Ishihara, R. Szalapski and D. Zeppenfeld, Phys. Rev. **D48**, 2182 (1993).

[77] C. Arzt, M. B. Einhorn and J. Wudka, Nucl. Phys. **B433**, 41 (1995), [hep-ph/9405214].

[78] M. C. Gonzalez-Garcia, Int. J. Mod. Phys. **A14**, 3121 (1999), [hep-ph/9902321].

[79] V. Barger, T. Han, P. Langacker, B. McElrath and P. Zerwas, Phys. Rev. **D67**, 115001 (2003), [hep-ph/0301097].

[80] B. Zhang, Y.-P. Kuang, H.-J. He and C. P. Yuan, Phys. Rev. **D67**, 114024 (2003), [hep-ph/0303048].

[81] U. Baur, T. Han and J. Ohnemus, Phys. Rev. **D51**, 3381 (1995), [hep-ph/9410266].

[82] J. Grosse-Knetter, M. Kobel, M. Mertens and M. Schumacher, ATLAS note, in preparation.

[83] O. J. P. Eboli, M. C. Gonzalez-Garcia, S. M. Lietti and S. F. Novaes, Phys. Rev. **D63**, 075008 (2001), [hep-ph/0009262].

[84] G. J. Gounaris, J. Layssac and F. M. Renard, Phys. Lett. **B332**, 146 (1994), [hep-ph/9311370].

[85] G. J. Gounaris, J. Layssac, J. E. Paschalis and F. M. Renard, Z. Phys. **C66**, 619 (1995), [hep-ph/9409260].

[86] V. D. Barger, K.-m. Cheung, A. Djouadi, B. A. Kniehl and P. M. Zerwas, Phys. Rev. **D49**, 79 (1994), [hep-ph/9306270].

[87] M. Kramer, J. H. Kuhn, M. L. Stong and P. M. Zerwas, Z. Phys. **C64**, 21 (1994), [hep-ph/9404280].

[88] K. Hagiwara and M. L. Stong, Z. Phys. **C62**, 99 (1994), [hep-ph/9309248].

[89] W. Kilian, M. Kramer and P. M. Zerwas, Phys. Lett. **B381**, 243 (1996), [hep-ph/9603409].

[90] J. F. Gunion, T. Han and R. Sobey, Phys. Lett. **B429**, 79 (1998), [hep-ph/9801317].

[91] K. Hagiwara, S. Ishihara, J. Kamoshita and B. A. Kniehl, Eur. Phys. J. **C14**, 457 (2000), [hep-ph/0002043].

[92] W. Kilian, LC-TOOL-2001-039; `http://www-ttp.physik.uni-karlsruhe.de/whizard`.

[93] T. Sjostrand, L. Lonnblad and S. Mrenna, hep-ph/0108264.

[94] T. Ohl, hep-ph/0011243.

[95] T. Ohl, hep-ph/0011287.

[96] M. Moretti, T. Ohl and J. Reuter, hep-ph/0102195.

[97] M. Pohl and H. J. Schreiber, hep-ex/0206009.

[98] F. James and M. Roos, Comput. Phys. Commun. **10**, 343 (1975).

[99] S. Catani, Y. L. Dokshitzer, M. H. Seymour and B. R. Webber, Nucl. Phys. **B406**, 187 (1993).

[100] J. M. Butterworth, J. P. Couchman, B. E. Cox and B. M. Waugh, Comput. Phys. Commun. **153**, 85 (2003), [hep-ph/0210022].

[101] M. Cacciari and G. P. Salam, hep-ph/0512210.

[102] S. Allwood, talk at the ATLAS physics week, Rome, 2005, `http://prorm3.roma3.infn.it/atlas/apw/`.

[103] S. Allwood, Ph.D. thesis, Manchester University (2006).

[104] S. Stefanidis, Ph.D. thesis, University College London (2006).

[105] M. S. Chanowitz, Czech. J. Phys. **55**, B45 (2005), [hep-ph/0412203].

[106] E. Accomando, A. Ballestrero, A. Belhouari and E. Maina, hep-ph/0603167.

[107] E. Accomando, A. Ballestrero and E. Maina, JHEP **07**, 016 (2005), [hep-ph/0504009].

[108] E. Accomando, A. Ballestrero and E. Maina, Nucl. Instrum. Methods **A534**, 265 (2004), [hep-ph/0404236].

[109] G. Cerminara, A Study of the WW-fusion Process at CMS as a Probe of Symmetry Breaking, Master's thesis, Turin University, `http://www.to.infn.it/~cerminar/documents/`

papers/03-07_tesi.pdf, 2003.

[110] R. Bellan, Observables in VV-fusion at the CMS Experiment, Master's thesis, Turin University, http://www.to.infn.it/~bellan/works/tesi/tesi_bellan.pdf, 2004.

[111] S. Bolognesi, Studio della rottura spontanea di simmetria mediante il processo di fusione di bosoni vettori nell'ambito dell'esperimento CMS, Master's thesis, Turin University, http://www.to.infn.it/~bolognes/docu/tesi_bolognesi.pdf.gz, 2005.

[112] A. De Roeck and H. Jung, editors, *HERA and the LHC—A Workshop on the Implications of HERA for LHC Physics: Proceedings, Part B* (2006), hep-ph/0601013.